Ground Based Studies of Thermocapillary Flows in Levitated Drops: Analytical Part

Final Report (April 1, 1993 – December 31, 1996)

Principal Investigator: S.S. Sadhal
Department of Mechanical Engineering
University of Southern California
Los Angeles, CA 90089–1453

Co-Investigator: Eugene H. Trinh
183–401 Jet Propulsion Laboratory
4800 Oak Grove
Pasadena, CA 91109

NASA Grant No.: NAGW–3378
Grants Officer: Dr. Bradley Carpenter

March 28, 1997

1 Objectives

The main objectives of the analytical part of this investigation are to study the fluid flow phenomena together with the thermal effects on drops levitated in an acoustic field. To a large extent, experimentation on ground requires a strong acoustic field that has a significant interference with other thermal-fluid effects. While most of the work has been directed towards particles in strong acoustic fields to overcome gravity, some results for microgravity have been obtained.

One of the objectives was to obtain the thermocapillary flow in a spot-heated drop, and set up a model for the prediction of thermophysical properties. In addition, for acoustically levitated particles, a clear understanding of the underlying fluid mechanics was required. Also, the interaction of acoustics with steady and pulsating thermal stimuli was required to be analyzed.

The experimental part of the work was funded through JPL, and has been reported separately.

2 Accomplishments

The analytical developments have led to several new and interesting results pertaining to heat transfer and fluid mechanics. A summary of each set of results is given here.

2.1 Thermocapillary Flow in a Spot-Heated Drop

In microgravity situations, the low Marangoni number flow for a spot-heated liquid drop has been analyzed. As a first approximation, heat flow treated as pure conduction. The liquid region is considered to be fully transient while the surrounding gas medium is regarded as quasisteady. From the analytical solution for the temperature distribution, the thermocapillary force on the interface was calculated and applied as an interface condition for Stokes flow in both the media. This led to the complete flow streamlines in the drop, as well as an expression for the migration velocity. The results have been presented for a liqiod-to-solid conductivity ratio of 100 and Fourier numbers ranging from 0.1 to 10. The inference of the the thermal diffusivity form the calculations have been discussed in the paper which has been accepted for publication in *Microgravity Science and Technology*, Vol. **X** (1997).

2.2 Acoustic Streaming Around a Sphere

For a particle levitated in an acoustic field, its position is determined, to some extent, by the compressibility properties of the particle phase relative to the surrounding medium. For example, liquid particles in a gas tend to position themselves at the velocity antinode while gas bubbles equilibrate at the velocity node. The effect of a gravity-type body

force may offset the equilibrium position to a point somewhere between the node and the antinode.

The fluid mechanics for the case of a particle at the velocity antinode can be derived directly from Riley's (1966) work for a vibrating sphere in an otherwise quiescent fluid. However, the flow about the velocity node has not been available and a detailed analysis for that situation has been carried out. In the present development, the perturbation procedure of Riley (1966) is employed to derive the flow field for the situation when a spherical particle is positioned at the velocity node. As in Riley's solution which applies to a sphere at the velocity antinode, it is found that there is a thin shear-wave region adjacent to the spherical boundary. However, for this thin Stokes layer, the streamlines are not closed but join with the outer flow. Therefore, the shear-wave layer does not cover the entire sphere as in the previous case, but lies mostly around the equatorial region of the sphere. The equatorial belt lies in the region $55° < \theta < 125°$.

Besides providing detailed knowledge about the flow field around the particle at the velocity node, the present analysis is very useful for developing the solution when the particle between the node and the antinode. This will be a combination of the two solutions along with some nonlinear interaction terms.

The velocity-node solution is to be submitted for publication. The work has been presented as a part of Ms. Hong Zhao's Ph.D. dissertation proposal.

2.3 Internal Circulation in a Drop in an Acoustic Field

The internal flow in a drop at the antinode of a standing wave has been investigated. This was done through the application of the stress continuity condition at the liquid-gas interface. To the leading order of calculation, the internal flow field was found to be very weak. At the next higher order, steady internal flows are predicted. There is, however, an important effect on the recirculating Stokes layer which vanishes when

$$|M| < \left(\tfrac{5}{2}\right)\sqrt{2}\,[2 + 5(\hat{\mu}/\mu)]\,,$$

where $\hat{\mu}$ is the liquid viscosity, μ is the exterior gas-phase viscosity, and M is the dimensionless frequency parameter for the gas phase, defined by

$$M = \frac{i\omega a^2 \rho}{\mu}.$$

This is a very interesting new development which needs detailed confirmation with experiments. While it agrees with many expriments with levitated drops where no recirculating layer has been found, a new set of experiments for specifically testing the theory need to be cerried out.

The work has also been presented as a part of Ms. Hong Zhao's Ph.D. dissertation proposal.

2.4 Thermoacoustic Streaming from a Sphere

This work consists of a study of the thermal effects of the steady streaming motion induced by a solid sphere. The thermal field is generated by an oscillating boundary condition on the surface of the sphere. The interesting feature here is that when the thermal frequency is 'in tune' with the acoustic field, the convective heat transfer term remains nonzero when the energy equation is averaged over time. This leads to a net flow of energy through the equatorial plane of the sphere.

A singular perturbation analysis has been carried out for small values of the streaming Reynolds number ($U_\infty / R\omega \ll 1$), along with $|M| = a^2\omega/\nu \gg 1$. There is equal heating and cooling of the regions above and below this plane, respectively. A result for the net flow across the equatorial plane of the sphere has been obtained.

The above case of thermoacoustic streaming has been extended to the case of pulsating spot heating. Again, the frequency of oscillation is in tune with the acoustic field and the time-averaged energy equation describes nonzero convective transport. The thermal energy deposited is divided between the solid sphere and the surrounding gas medium on the basis of the respective thermal transport characteristics. The calculations have provided an analytical expression for the transient thermal field. The analysis for long times (large Fourier number) predicts steady buildup of the time-averaged temperature in the sphere. While experimentation with thermoacoustics has shown somewhat similar behavior, there is some skepticism about the present prediction which could perhaps be an artifact of approximation.

A paper (Gopinath & Sadhal, 1994) resulting from this work has been published in the Proceedings of the 1994 International Heat and Mass Transfer Conference (Brighton, UK).

3 Microgravity Sessions in ASME Conferences

The Principal Investigator has taken a role in organizing technical sessions the National Heat Transfer Conference and the International Mechanical Engineering Congress and Exposition under the auspicies of the American Society of Mechanical Engineers. The following sessions were organized and chaired by the P.I.:

1. Heat Transfer in Microgravity Systems, 29th National Heat Transfer Conference, Atlanta, August 8–11, 1993.

2. Heat Transfer in Microgravity Systems, International Mechanical Engineering Congress & Exposition, Chicago, November 6–11, 1994.

3. Heat Transfer in Microgravity Systems, 30th National Heat Transfer Conference, Portland, Oregon, August 6–8, 1995.

4. Heat Transfer in Microgravity Systems, International Mechanical Engineering Congress & Exposition, San Francisco, November 11–17, 1995.

5. Heat Transfer in Microgravity Systems, International Mechanical Engineering Congress & Exposition, Atlanta, November 17–22, 1996.

4 Publications & Presentations

4.1 Journal Papers

1. Sadhal, S.S., Trinh, E.H. & Wagner, P., "Unsteady Spot Heating of a Drop in a Microgravity Environment," *Microgravity Science and Technology*, in press (1997).

2. Zhao, H., Sadhal, S.S., & Trinh, E.H., "Singular Perturbation Analysis of an Acoustically Levitated Sphere: Flow About the Velocity Node," submitted, *Phys. Fluids* (1997).

4.2 Conference Proceedings

1. Gopinath, A. & Sadhal, S.S., "Thermoacoustic Streaming Effects from a Sphere Subject to Time-Periodic Temperature Disturbances," accepted, Tenth International Heat & Mass Transfer Conference, Brighton, U.K., August 1994.

2. Trinh, E.H. & Sadhal, S.S., "Acoustic Streaming and Ultrasonic Processing of Low Melting Point Materials," 1994 Int. Mech. Eng. Congress, Chicago, November 6–11, 1994. In *Heat Transfer in Microgravity Systems 1994*, ASME HTD-Vol. 290, pp 43–52.

3. E. H. Trinh & S. S. Sadhal, "Visualization of Internal Flows in Differentially Heated Drops," Gordon Conference on Gravitational Effects in Physico-Chemical Systems, July 1995.

4.3 Book

Sadhal, S.S., Ayyaswamy, P.S., & Chung, J.N., *Transport Phenomena with Drops and Bubbles*, Springer-Verlag, 520 pages, 1997, ISBN 0-387-94678-0. This monograph includes a chapter dealing with thermocapillary phenomena with drops and bubbles.

4.4 Edited Works

1. S.S. Sadhal, A. Gopinath, P.D. Jones, J. Seyed-Yagoobi, & K.A. Woodbury, *Proceedings of the the ASME Heat Transfer Division – Volume 1*, American Society of Mechanical Engineers, No. HTD–332, ISBN 0-7918-1519-6 (1996).

2. S.S. Sadhal, A. Gopinath, P.H. Oosthuisen & A. Hashemi, *Proceedings of the 30th National Heat Transfer Conference – Volume 3*, American Society of Mechanical Engineers, No. HTD–305, ISBN 0-7918-1704-0 (1995).

3. S.S. Sadhal & A. Gopinath, *Heat Transfer in Microgravity Systems 1994*, American Society of Mechanical Engineers, No. HTD–290, ISBN 0-7918- 1408-4 (1994).

4. S.S. Sadhal & A. Hashemi, *Heat Transfer in Microgravity Systems 1993*,

   American Society of Mechanical Engineers, No. HTD–235, ISBN 0-7918- 1148-4 (1993).

4.5 Invited Lecture

"Fluid Flow and Thermal Transport with Acoustically Levitated Spheres," presented at *"Gotas, burbujas y películas (Drops Bubbles, & Films)"*, Escuela de Físico–Química de Fluidos, Santander, Spain, September 9–13, 1996.

S. S. Sadhal, E. H. Trinh and P. Wagner

Thermocapillary Flows in a Drop With Unsteady Spot Heating in a Microgravity Environment

The unsteady localized spot heating of a liquid drop under zero-g conditions is examined theoretically. This pertains to space experiments to measure thermal properties of materials and the purpose here is to predict the thermal behavior of such systems. Spot heating can be achieved by a laser beam focused on a small region of the drop surface. The present theoretical model deals with situations of weak Marangoni flows, whereby the thermal transport is conduction dominated. The heat flow in the drop is treated as unsteady while the surrounding gaseous region is considered to be quasi-steady. The ensuing thermally driven flow is analyzed in the Stokes regime.

1 Introduction

Since the availability of experimental facilities in space, studies in low-gravity environments have gained considerable attention. Much of the interest in the last decade started with some pioneering papers of *Subramanian* and *Weinberg* [1, 2]. One of the principal advantages of a low gravity situation is that deep undercooling of liquids is possible because of fluid being undisturbed. In this context, it is of fundamental interest to acquire information about the thermophysical properties of the liquids in undercooled states. To this end, various low-*g* experiments have been proposed. Among them is the idea of spot heating a spherical sample of the liquid under test in zero, or low gravity (see fig. 1). This idea was proposed by *Subramanian* (see [3, 4]) more than a decade ago but analytical studies have only been recently conducted. A laser beam can be used to heat a small fraction of the drop surface. The thermal field thus developed will lead to Marangoni convection and the observation of the fluid motion can be used to infer the thermal properties of the sample. This possible use of method has also been investigated by *Shen* and *Khodadadi* [5, 6].

Mail address: S.S. Sadhal, Department of Mechanical Engineering, University of Southern California, Los Angeles, CA 90089-1453, USA, E.H. Trinh and P. Wagner, Jet Propulsion Laboratory, Pasadena, CA 91109, USA.
Paper submitted: June 15, 1995
Submission of final revised version: November 13, 1996
Paper accepted: December 2, 1996

Since the low gravity significantly weakens the natural convection phenomenon, Marangoni convection becomes isolated and it is the dominant mode of thermally driven motion. The study of Marangoni convection under microgravity condition has been the subject of considerable study in the last several years, particularly in relation to drops and bubbles. Among the major theoretical works are the investigations by *Annamalai* et al. [3], *Barton* and *Subramanian* [7–9], *Kim* and *Subramanian* [10, 11], *Merritt* and *Subramanian* [12, 13], *Meyyappan* et al. [14–17], and *Shankar* and *Subramanian* [18]. They have also addressed a number of problems involving compound drops. For spherically concentric systems, *Bauer* and *Eidel* [19] obtained three-dimensional solutions for a class of thermocapillary flows. They examined various configurations including the case of a drop within a drop with a rigid outer boundary and full continuity at the inner interface. In addition, they treated the situation of a rigid inner boundary with a free outer interface. The thermocapillary migration of a drop heated by radiation on one side has been analyzed in the steady state by *Oliver* and *DeWitt* [20]. They obtained an expression for the migration velocity as a function of a radiative intensity. Reviews of work on thermocapillary flows in microgravity are available in [21–23].

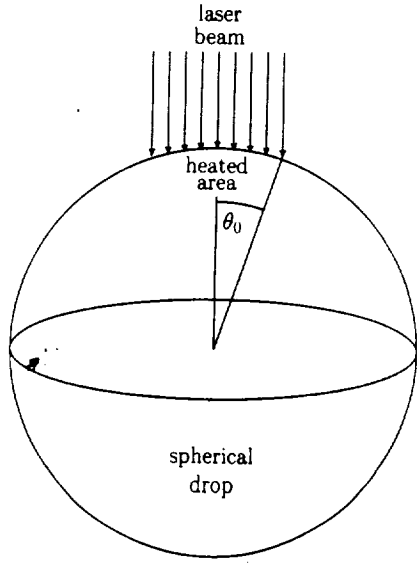

Fig. 1. A schematic of a spherical drop being spot heated

Much of the earlier work has focused on drops and bubbles in a linear temperature profile and there has been little effort in the direction of spot heating. The present analysis is directed towards the study of the thermal and the fluid dynamical effects of spot heating on a liquid drop. The Marangoni convection is considered to be weak enough so that the convective transport of heat may be neglected.

Thus pure conduction dominates in the liquid phase, as well as in the surrounding gas phase. The drop is treated as fully transient, but the gas, owing to its low heat capacity, can be analyzed in the quasisteady state. This assumption limits the validity to cases for which the liquid thermal diffusivity is much lower than that of the gas. For most glass-like materials in a gas, this is often the case. For example, the thermal diffusivity of glass is approximately $6 \cdot 10^{-7}\ \mathrm{m^2\,s^{-1}}$, while that for air at 20 °C is about $2 \cdot 10^{-5}\ \mathrm{m^2\,s^{-1}}$. The fluid flow is considered to be inertialess due to the high viscosity of the dispersed phase together with the weak thermal driving force. This corresponds to a low Marangoni number which is defined as

$$Ma = \frac{\hat{Q}}{\hat{k}\hat{\mu}\hat{\alpha}}\left(-\frac{\mathrm{d}\sigma}{\mathrm{d}T}\right), \tag{1}$$

where $\hat{Q}$ is the power of the laser; $\hat{k}$, $\hat{\alpha}$, and $\hat{\mu}$ correspond to the thermal conductivity, the thermal diffusivity, and the kinematic viscosity, respectively, of the liquid drop; and σ is the interfacial tension. For glassmelts, we take the estimate given in table 1 of the thermophysical parameters near the solidification state [24].

Here, the upper limit of the viscosity is near the 'transformation temperature' in an undercooled state [24]. Taking $\hat{\mu}$ to be $10^3\ \mathrm{N\,s\,m^{-2}}$, for Ma to be between the range 10^{-2} to 10^{-3}, $\hat{Q}$ should be about 0.6 to 6 mW. This power level is enough to set off an observable motion and yet keep $Ma \ll 1$. At higher viscosity values of the melt, the power level can be raised to obtain an observable motion.

In the gaseous continuous phase, while the dynamic viscosity may be low, the kinematic viscosity ($\nu = \mu/\varrho$) is large because of the low gas-phase density. The flow field is considered to be quasi-steady under the low Reynolds number approximation, i.e., the time derivatives in the Navier–Stokes equation are dropped. This is usually done for Stokes flow because the diffusion time scale, $R^2/\hat{\nu}$, is much smaller than the dynamic time scale, R/U. This is consistent with the assumption, $Re \ll 1$. The drop deformation is also considered to be negligible because the normal stress forces arising from the surface tension variation and the fluid motion are similar in magnitude as the Marangoni forces.

The flow observations coupled with some thermal measurements near the drop will provide sufficient data to acquire information about the thermal properties of the liquid under test. The transient evolution of the quasi-steady flow field prediction may be compared with the experimental measurements and thermal diffusivity information can be derived. The dominant transient is the heat diffusion in the liquid drop. This assumption realistically limits the validity to cases where $\hat{\alpha} \ll \alpha, \hat{\nu}, \nu$. The observation of the evolution of the central ring of the toroidal vortex will provide information about the thermal diffusivity. While the flow equations are time-dependent, the temporal evolution appears in a quasi-steady manner, as just mentioned, because the interface conditions are time-dependent.

2 Statement of Problem

The mathematical model consists of a liquid drop of radius R surrounded by an infinite gaseous medium. A laser beam is focused on a small area of the drop surface. The gas is considered to be transparent to the radiation which is absorbed at the surface with some reflected back and negligible penetration into the liquid. Thus the heated spot behaves as a surface source of heat. In the absence of any other driving force, the problem is symmetric about the axis of the beam. As stated earlier, we assume that the thermal diffusivity of the liquid is much smaller than that of the gas.

We use the notation where the quantities corresponding to the drop are referred to with a hat (^). Thus, assuming $\hat{\alpha} \ll \alpha$ and neglecting convective transport, we have the temperature fields described by

$$\frac{1}{\alpha}\frac{\partial \hat{T}}{\partial t} = \frac{\partial^2 \hat{T}}{\partial r^2} + \frac{2}{r}\frac{\partial \hat{T}}{\partial r} + \frac{1}{r^2 \sin(\theta)}\frac{\partial}{\partial \theta}\left(\sin(\theta)\frac{\partial \hat{T}}{\partial \theta}\right), \tag{2}$$

and

$$0 = \frac{\partial^2 T}{\partial r^2} + \frac{2}{r}\frac{\partial T}{\partial r} + \frac{1}{r^2 \sin(\theta)}\frac{\partial}{\partial \theta}\left(\sin(\theta)\frac{\partial T}{\partial \theta}\right). \tag{3}$$

The continuity conditions at the interface are

$$\hat{T}|_{r=R} = T|_{r=R} \tag{4}$$

and

$$\left[\hat{k}\frac{\partial \hat{T}}{\partial r} - k\frac{\partial T}{\partial r}\right]_{r=R} = \begin{cases} q_0 \cos(\theta) & 0 < \theta < \theta_0, \\ 0 & \theta_0 < \theta < \pi, \end{cases} \tag{5}$$

where q_0 is the net heat flux deposited by the laser beam. This is distributed somewhat unevenly because of the surface curvature and this effect introduces the factor $\cos(\theta)$. However, it is a minor issue from a practical standpoint because the laser intensity is seldom uniform.

In the far field, the temperature is uniform, i.e.,

$$T \to T_\infty \quad \text{as} \quad r \to \infty. \tag{6}$$

The initial condition is

$$\hat{T} = T = T_\infty \quad \text{at} \quad t = 0. \tag{7}$$

The differential equations for the fluid velocity can be reduced to a scalar form in the usual manner with the use

Table 1. Properties of liquid glass near the solidification state

$\hat{k}$	$\hat{\mu}$	$\hat{\alpha}$	σ_0	$\mathrm{d}\sigma/\mathrm{d}T$
$1.0\ \mathrm{W\,m^{-1}\,K^{-1}}$	$10^3 - 10^{12.3}\ \mathrm{N\,s\,m^{-2}}$	$6 \cdot 10^{-7}\ \mathrm{m^2\,s^{-1}}$	$300\ \mathrm{N\,m^{-1}}$	$-10^{-3}\ \mathrm{N\,m^{-1}\,K^{-1}}$

of the Stokes stream functions, i.e.,

$$u_r = \frac{1}{r^2 \sin(\theta)} \frac{\partial \psi}{\partial \theta}, \quad u_\theta = \frac{-1}{r \sin(\theta)} \frac{\partial \psi}{\partial r}, \tag{8}$$

and

$$\hat{u}_r = \frac{1}{r^2 \sin(\theta)} \frac{\partial \hat{\psi}}{\partial \theta}, \quad \hat{u}_\theta = \frac{-1}{r \sin(\theta)} \frac{\partial \hat{\psi}}{\partial r}, \tag{9}$$

The stream functions, ψ and $\hat{\psi}$ obey

$$L^2_{-1}\psi = 0, \quad \text{and} \quad L^2_{-1}\hat{\psi} = 0, \tag{10}$$

respectively. Here,

$$L_{-1} = \frac{\partial^2}{\partial r^2} + \frac{\sin(\theta)}{r^2} \frac{\partial}{\partial \theta}\left(\frac{1}{\sin(\theta)} \frac{\partial}{\partial \theta}\right) \tag{11}$$

is the Stokes operator. On the interface $r = R$, normal velocity is zero, and the tangential velocity is continuous. There is a tangential stress discontinuity that is equal to the surface tension gradient, $(1/R)(\partial\sigma/\partial\theta)$. These interface conditions may be written as

$$\psi|_{r=R} = \hat{\psi}|_{r=R} = 0, \tag{12}$$

$$\left.\frac{\partial \psi}{\partial r}\right|_{r=R} = \left.\frac{\partial \hat{\psi}}{\partial r}\right|_{r=R}, \tag{13}$$

and

$$\frac{1}{R}\frac{d\sigma}{dT}\left(\frac{\partial T}{\partial \theta}\right)_{r=R} = [\tau_{r\theta} - \hat{\tau}_{r\theta}]_{r=R}$$
$$= -\left[\mu \frac{r}{\sin(\theta)} \frac{\partial}{\partial r}\left(\frac{1}{r^2}\frac{\partial \psi}{\partial r}\right) - \hat{\mu} \frac{r}{\sin(\theta)} \frac{\partial}{\partial r}\left(\frac{1}{r^2}\frac{\partial \hat{\psi}}{\partial r}\right)\right]_{r=R}, \tag{14}$$

where μ is the gas phase viscosity and $\hat{\mu}$ is that for the liquid. In addition, we must have finite velocity at the origin. This is satisfied by

$$\frac{1}{r^2}\hat{\psi} < \infty \quad \text{as} \quad r \to 0. \tag{15}$$

3 Solution

The solution consists of the determination of the temperature field and the ensuing velocity field.

3.1 The Temperature Field

The solution for the temperature distribution can be easily obtained by Laplace transform. Taking the Laplace transform of the set of differential equations (1)–(6) we obtain:

$$\frac{1}{\hat{\alpha}}(s\hat{T} - T_\infty) = \frac{\partial^2 \hat{T}}{\partial r^2} + \frac{2}{r}\frac{\partial \hat{T}}{\partial r} + \frac{1}{r^2}\frac{\partial}{\partial \eta}(1-\eta^2)\frac{\partial \hat{T}}{\partial \eta} \tag{16}$$

$$0 = \frac{\partial^2 \bar{T}}{\partial r^2} + \frac{2}{r}\frac{\partial \bar{T}}{\partial r} + \frac{1}{r^2}\frac{\partial}{\partial \eta}(1-\eta^2)\frac{\partial \bar{T}}{\partial \eta} \tag{17}$$

$$\hat{T}|_{r=R} = \bar{T}|_{r=R}, \tag{18}$$

$$\left[\phi_k \frac{\partial \hat{T}}{\partial r} - \frac{\partial \bar{T}}{\partial r}\right]_{r=R} = \begin{cases} \dfrac{q_0 \eta}{ks}, & \eta_0 < \eta < 1 \\ 0 & -1 < \eta < \eta_0, \end{cases} \tag{19}$$

where $\eta = \cos(\theta)$, $\eta_0 = \cos(\theta)_0$ and $\phi_k = \hat{k}/k$. The solutions to these differential equations can be written as

$$\hat{T} = \sum_{n=0}^{\infty} a_n i_n(qr) P_n(\eta) + \frac{T_\infty}{s}, \tag{20}$$

$$\bar{T} = \sum_{n=0}^{\infty} a_n \left(\frac{R}{r}\right)^{n+1} i_n(qR) P_n(\eta) + \frac{T_\infty}{s}, \tag{21}$$

where $i_n(qr)$ represents modified spherical Bessel functions and

$$q = \left(\frac{s}{\hat{\alpha}}\right)^{1/2}.$$

To satisfy the boundary condition (19) we expand the right hand side, so that

$$\sum_{n=0}^{\infty} a_n \left\{\phi_k q i_n'(qR) + i_n(qR)\frac{(n+1)}{R}\right\} P_n(\eta) = \frac{q_0}{ks}\sum_{n=0}^{\infty} H_n P_n(\eta),$$

where

$$H_n = (n+\tfrac{1}{2})\int_{\eta_0}^{1} \eta P_n(\eta)\, d\eta$$
$$= \frac{(n+\frac{1}{2})(1-\eta_0^2)[\eta_0 P_n'(\eta_0) - P_n(\eta_0)]}{(n+2)(n-1)}, \quad (n \neq 1),$$

$$H_1 = \tfrac{1}{2}(1-\eta_0^3).$$

As a result we obtain

$$a_n = \left(\frac{q_0 R}{ks}\right)\frac{H_n}{[q\phi_k R i_n'(qR) + (n+1) i_n(qR)]}.$$

Therefore, we have

$$\hat{T}(r,\eta) = \left(\frac{q_0 R}{ks}\right)\sum_{n=0}^{\infty}\frac{H_n i_n(qr) P_n(\eta)}{[q\phi_k R i_n'(qR) + (n+1) i_n(qR)]} + \frac{T_\infty}{s}$$

and

$$\bar{T}(r,\eta) = \left(\frac{q_0 R}{ks}\right)\sum_{n=0}^{\infty}\frac{H_n i_n(qR)(R/n)^{n+1} P_n(\eta)}{[q\phi_k R i_n'(qR) + (n+1) i_n(qR)]} + \frac{T_\infty}{s}.$$

Inversion of the Laplace transform yields

$$\hat{T} - T_\infty = \left(\frac{q_0 R}{k}\right)$$
$$\cdot \sum_{n=0}^{\infty}\left\{\sum_{m=1}^{\infty}\frac{2\phi_k [j_n(\lambda_{mn} r)/j_n(\lambda_{mn} R)]\, e^{-\hat{\alpha}\lambda_{mn}^2 t}}{(n+1)[n\phi_k^2 + \phi_k - (n+1)] - \lambda_{mn}^2 R^2 \phi_k^2} + \frac{(r/R)^n}{n\phi_k + (n+1)}\right\} H_n P_n(\cos(\theta)), \tag{22}$$

and

$$T - T_\infty = \left(\frac{q_0 R}{k}\right)$$
$$\cdot \sum_{n=0}^{\infty}\left\{\sum_{m=1}^{\infty}\frac{2\phi_k\, e^{-\hat{\alpha}\lambda_{mn}^2 t}}{(n+1)[n\phi_k^2 + \phi_k - (n+1)] - \lambda_{mn}^2 R^2 \phi_k^2} + \frac{1}{n\phi_k + (n+1)}\right\}\left(\frac{R}{r}\right)^{n+1} H_n P_n(\cos(\theta)), \tag{23}$$

where λ_{mn} represents the characteristic values given by the roots of

$$-\phi_k \lambda_{mn} R j_n'(\lambda_{mn} R) = (n+1) j_n(\lambda_{mn} R), \tag{24}$$

and $j_n(x)$ represents spherical Bessel functions.

3.2 The Velocity Field

The stream functions represented by the solutions of equation (10) are given as [25]

$$[\psi(r,\theta), \hat{\psi}(r,\theta)] = \sum_{n=1}^{\infty} [a_n r^{n+3} + b_n r^{n+1} + c_n r^{-n+2} + d_n r^{-n}] \int_{\cos(\theta)}^{1} P_n(x)\,dx. \tag{25}$$

Upon satisfying the boundary and interface conditions (12), (13), and (15), the above general solution reduces to

$$\hat{\psi}(r,\theta) = \sum_{n=1}^{\infty} C_n(t)\left[\left(\frac{r}{R}\right)^{n+3} - \left(\frac{r}{R}\right)^{n+1}\right] \int_{\cos(\theta)}^{1} P_n(x)\,dx \tag{26}$$

and

$$\psi(r,\theta) = \sum_{n=1}^{\infty} C_n(t)\left[\left(\frac{r}{R}\right)^{-n+2} - \left(\frac{r}{R}\right)^{-n}\right] \int_{\cos(\theta)}^{1} P_n(x)\,dx. \tag{27}$$

Applying the tangential stress jump condition,

$$\frac{1}{R}\frac{\partial \sigma}{\partial \theta} = [\tau_{r\theta} - \hat{\tau}_{r\theta}]_{r=R} = -\left[\mu \frac{r}{\sin(\theta)}\frac{\partial}{\partial r}\left(\frac{1}{r^2}\frac{\partial \psi}{\partial r}\right) - \hat{\mu}\frac{r}{\sin(\theta)}\frac{\partial}{\partial r}\left(\frac{1}{r^2}\frac{\partial \hat{\psi}}{\partial r}\right)\right]_{r=R}, \tag{28}$$

we obtain

$$\frac{\partial \sigma}{\partial \theta} = \frac{2(\mu+\hat{\mu})}{R^2}\sum_{n=1}^{\infty} C_n(t)(2n+1)\frac{\sin(\theta)}{n(n+1)} P_n'(\cos(\theta)). \tag{29}$$

Now, using

$$\frac{\partial \sigma}{\partial \theta} = \frac{d\sigma}{dT}\left(\frac{\partial T}{\partial \theta}\right)_{r=R} \tag{30}$$

and

$$\left(\frac{\partial T}{\partial \theta}\right)_{r=R} = \left(\frac{2q_0 R}{k}\right) \sum_{m=1}^{\infty}\sum_{n=0}^{\infty} \frac{H_n P_n'(\cos(\theta))(-\sin(\theta))\phi_k\, e^{-\hat{\kappa}\lambda_{mn}^2 t}}{(n+1)[n\phi_k^2 + \phi_k - (n+1)] - \lambda_{mn}^2 R^2 \phi_k^2} + \frac{q_0 R}{\hat{k}}\sum_{n=0}^{\infty}\frac{H_n P_n'(\cos(\theta))(-\sin(\theta))}{n\phi_k + (n+1)} \tag{31}$$

find that

$$C_n(t) = -\left[\frac{q_0 R^3}{2(\mu+\hat{\mu})\hat{k}}\right]\left(\frac{d\sigma}{dT}\right) \cdot \left\{\sum_{m=1}^{\infty} \frac{2e^{-\hat{\kappa}\lambda_{mn}^2 t}}{(n+1)[n+\phi_k - \phi_k^2(n+1)] - \lambda_{mn}^2 R^2} + \frac{1}{n+\phi_k(n+1)}\right\} H_n\left[\frac{n(n+1)}{2n+1}\right]. \tag{32}$$

3.3 Thermocapillary Force and Drop Migration

The force experienced by the drop is proportional to the strength of the stokeslet, and is given by

$$F = \frac{4\pi\mu C_1}{R}. \tag{33}$$

which has the steady state value

$$F_{ss} = \left[\frac{2\pi q_0 R^2(1-\eta_0^3)}{3(1+\phi_\mu)(2+\phi_k)k}\right]\left(-\frac{d\sigma}{dT}\right). \tag{34}$$

Therefore, the thermocapillary force would cause the drop to move, unless an additional neutralizing force is present. Such a force can come about by means of a weak acoustic field, or an electrostatic field. For such a situation it is, of course, understood that the secondary flows arising from the neutralizing force are negligible, and the consequent limits of validity apply. In the absence of such a force, the migration velocity can be obtained by simply adding the Rybczynski–Hadamard velocity field to the solution given by eqs. (26) and (27). That is, for a migration velocity, U, we add on

$$\psi_0(r,\theta) = \frac{1}{2}UR^2\left\{\left(\frac{r}{R}\right)^2 - \left(\frac{R}{r}\right) - \frac{2+3\phi_\mu}{2(1+\phi_\mu)}\left[\left(\frac{r}{R}\right) - \left(\frac{R}{r}\right)\right]\right\}\sin^2(\theta), \tag{35}$$

and

$$\hat{\psi}_0(r,\theta) = \frac{1}{2}UR^2\left\{\frac{1}{2(1+\phi_\mu)}\right\}\left[\left(\frac{r}{R}\right)^4 - \left(\frac{r}{R}\right)^2\right]\sin^2(\theta), \tag{36}$$

to $\psi(r,\theta)$ and $\hat{\psi}(r,\theta)$, respectively, and require that the net force on the system be equal to zero. This is achieved by letting the term proportional to $(r\sin^2(\theta))$ vanish. As a result, the following expression for the migration velocity is obtained:

$$U = \frac{C_1}{R^2}\left[\frac{2(1+\phi_\mu)}{2+3\phi_\mu}\right]. \tag{37}$$

It has the steady state value,

$$U_{ss} = \left[\frac{q_0 R(1-\eta_0^3)}{3k\mu(2+3\phi_\mu)(2+\phi_k)}\right]\left(-\frac{d\sigma}{dT}\right), \tag{38}$$

which is consistent with the result of *Oliver* and *DeWitt* [20] for the special case of $\theta_0 = \frac{1}{2}\pi$.

3.4 Drop Deformation

Upon integrating eq. (29), the surface tension distribution is found to be

$$\sigma(\theta) = \sigma_0 - \frac{2(\mu + \hat{\mu})}{R^2} \sum_{n=1}^{\infty} C_n(t)\left[\frac{2n+1}{n(n+1)}\right] P_n(\cos(\theta)). \quad (39)$$

Following *Sadhal, Ayyaswamy* and *Chung* [21], the deformation may be expressed as

$$R(\theta) = R_0[1 + \zeta(\theta)], \quad (40)$$

where

$$\zeta(\theta) = -\frac{2(\mu + \hat{\mu})}{\sigma_0 R^2} \sum_{n=2}^{\infty} \frac{C_n(t)}{n(n+1)}\left[\frac{\phi_\mu}{(n+2)} + \frac{1}{(n-2)}\right] P_n(\cos(\theta)), \quad (41)$$

and R_0 is the radius of the isothermal drop. The surface tension of the liquid at the reference isothermal state is denoted by σ_0. By using the expression for $C_n(t)$, it is not difficult to see that

$$\zeta(\theta) = \frac{q_0 R_0}{\sigma_0 \hat{k}}\left(\frac{d\sigma}{dT}\right) \sum_{n=2}^{\infty} \left\{ \sum_{m=1}^{\infty} \frac{2e^{-\lambda_{mn}^2 t}}{(n+1)[n + \phi_k - \phi_k^2(n+1)] - \lambda_{mn}^2 R^2} + \frac{1}{n + \phi_k(n+1)} \right\} H_n \left[\frac{\phi_\mu}{(n+2)} + \frac{1}{(n-2)}\right] P_n(\cos(\theta)). \quad (42)$$

Here, considering $\dot{Q} = 0.1$ to 10 mW, a beam radius of 1 mm, a drop radius $R_0 = 5$ mm, and other properties as given in table 1, the dimensionless parameter in front of the above expression for $\zeta(\theta)$ is approximately given by

$$\frac{q_0 R_0}{\sigma_0 \hat{k}}\left(\frac{d\sigma}{dT}\right) \sim 10^{-5} \text{ to } 10^{-7}. \quad (43)$$

It is therefore easy to see that for the estimated set of glass properties, the drop deformation is very small.

4 Results and Discussion

The important results from this analysis consist of the temperature field and the flow streamlines. A computer program was written in FORTRAN to run on the *Cray Y-MP* at JPL. The program carries out the formulation in stages. At the first stage the roots, λ_{mn}, of the characteristic eq. (24) are obtained by the regula falsi method. For accuracy, the Legendre polynomials and their derivatives are evaluated using recurrence relations at higher orders rather than using polynomial expressions. The spherical Bessel functions are treated differently according to whether

(1) the square of the argument is very small compared with the order, in which case an expansion in this ratio is used;
(2) the order is greater than 3, in which case backward recurrence from an order based on the desired accuracy is used;
(3) otherwise, simple expressions with sines and cosines are used.

Because more terms are required for convergence of the steady-state solution than for convergence of the transient response, each is tested separately. The results are displayed as isotherms and streamlines using standard NCAR graphics library routines.

The temperature is scaled with the parameter, $q_0 R/\hat{k}$, and the calculations have been carried out at Fourier number values, $Fo = \hat{\alpha} t/R^2 = 0.1, 0.2, 0.5, 1, 2, 10$. The heated spot is defined by the angle, $\theta_0 = 15°$, as shown in fig. 1. For each case, the isotherms and the flow streamlines are given in figs. 2a–f. The diffusion of the heat can be seen progressing in time, as one set of isotherms is compared with the next.

The flow streamlines exhibit a single vortex arising purely from the thermally driven motion. The center of the vortex is away from the equatorial plane and finds a position toward the heated spot. A similar shift was found by *Oliver*

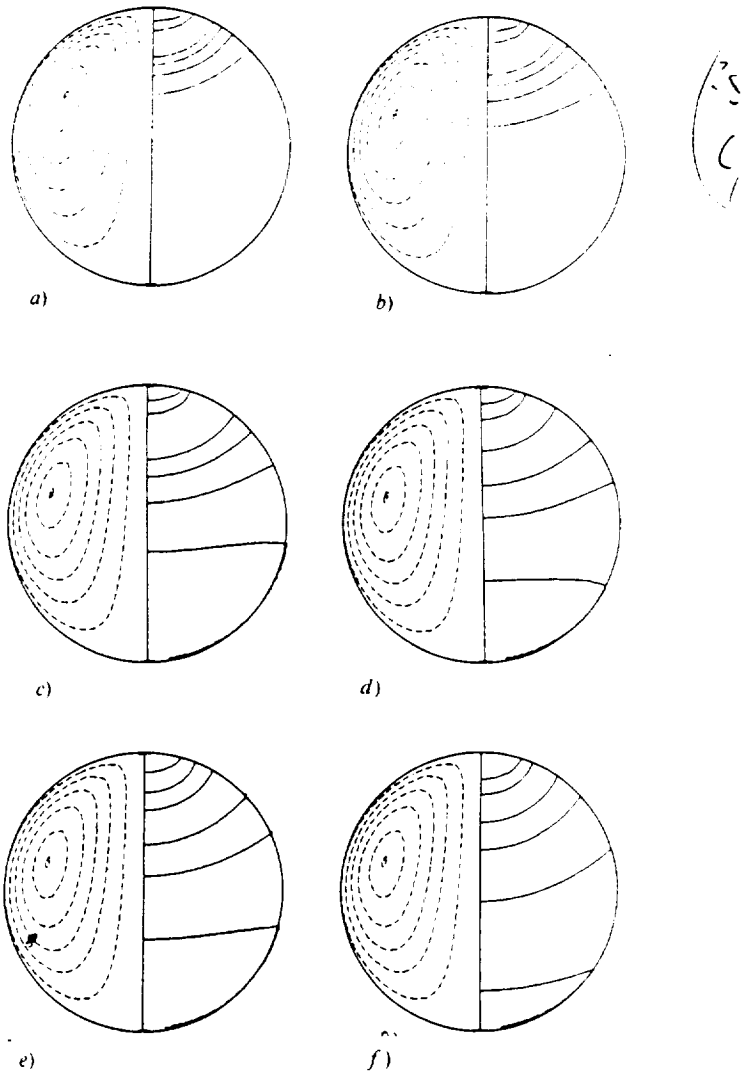

Fig. 2. Flow streamlines for a spot-heated drop. $\phi_k = 100$, $\theta_0 = 15°$, (a) $Fo = 0.1$, (b) $Fo = 0.2$, (c) $Fo = 0.50$, (d) $Fo = 1.0$, (e) $Fo = 2.0$, (f) $Fo = 10.0$

and *DeWitt* [20] for the case of a drop heated by radiation over half of the free surface. In the present analysis we find that as the thermal diffusion progresses, the vortex center shifts towards the equator. The position of the vortex center can be used to infer the thermal diffusivity of the test liquid. The usefulness of this approach is particularly evident because the streamlines are independent of the liquid and the gas viscosities at the present level of approximation.

List of Symbols

$i_n(x)$	modified spherical Bessel function
$j_n(x)$	spherical Bessel function
L_{-1}	Stokes operator
Ma	Marangoni number, $\hat{Q}(-d\sigma/dT)/(k\hat{\mu}\hat{\alpha})$
$P_n(x)$	Legendre polynomials
$\hat{Q}$	laser beam power [W]
q	$(s/\hat{\alpha})^{1/2}$
q_0	heat flux
r	radial coordinate
R	radius of the drop
s	Laplace transform parameter
t	time
T	temperature
u_r, u_θ	velocity components
α	thermal diffusivity
θ	polar angle
θ_0	angle subtended by heated area
μ	dynamic viscosity
η	cos (θ)
σ	interfacial tension
$\tau_{r\theta}$	shear stress
ϕ_k	conductivity ratio, $(\hat{k}/k)$
ψ	stream function
∞	far field (subscript)
$\bar{T}$	Laplace transform of T
$(\hat{})$	dipersed phase quantities

Acknowledgements

Support of this work by the U.S. National Aeronautics and Space Administration (Grant Nos. NAGW-3378 and NAG3-1842) is gratefully acknowledged.

References

1 *Subramanian, R. S., Weinberg, M. C.*: The Role of Convective Transport in Dissolution or Growth of a Gas Bubble. J. Chem. Phys., vol. 72, p. 6811 (1980)
2 *Subramanian, R. S., Weinberg, M. C.*: Asymptotic Expansions for the Description of Gas Bubble Dissolution and Growth. AIChE Journal, vol. 27, p. 739 (1981)
3 *Annamalai, P., Shankar, N., Cole, R., Subramanian, R. S.*: Bubble Migration Inside a Liquid Drop in a Space Laboratory. Appl. Sci. Res., vol. 38, p. 179
4 *Subramanian, R. S.*: Applications in the Academic and Scientific Community. IBM: Perspectives in Computing, Vol. 4, No. 2/3 (1984)
5 *Shen, F., Khodadadi, J. M.*: Transient Marangoni Convection Inside a Liquid Droplet. APS Bulletin, vol. 39, p. 1841 (1994)
6 *Shen, F., Khodadadi, J. M.*: An Extended Laser Flash Technique for Thermal Diffusivity Measurement of High Temperature Materials; in: NASA Conference Publication 10121, 1992. Workshop on Thermophysical Properties of Molten Materials, Cleveland, OH, p. 203 (1993)
7 *Barton, K. D., Subramanian, R. S.*: Thermocapillary Migration of a Liquid Drop Normal to a Plane Surface. J. Colloid Interface Sci., vol. 137, p. 170 (1990)
8 *Barton, K. D., Subramanian, R. S.*: The Migration of Liquid Drops in a Vertical Temperature Gradient. J. Colloid Interface Sci., vol. 133, p. 211 (1989)
9 *Barton, K. D., Subramanian, R. S.*: Migration of Liquid Drops in a Vertical Temperature Gradient – Intersection Effects Near a Horizontal Surface. J. Colloid Interface Sci., vol. 141, p. 146 (1991)
10 *Kim, H. S., Subramanian, R. S.*: Thermocapillary Migration of a Droplet With Insoluble Surfactant. I: Surfactant Cap. J. Colloid Interface Sci., vol. 127, p. 417 (1989)
11 *Kim, H. S., Subramanian, R. S.*: Thermocapillary Migration of a Droplet With Insoluble Surfactant. II: General Case. J. Colloid Interface Sci., vol. 130, p. 112 (1989)
12 *Merritt, R. M., Subramanian, R. S.*: The Migration of Isolated Gas Bubbles in a Vertical Temperature Gradient. J. Colloid Interface Sci., vol. 125, p. 333 (1988)
13 *Merritt, R. M., Subramanian, R. S.*: Migration of a Gas Bubble Normal to a Plane Horizontal Surface In a Vertical Temperature Gradient. J. Colloid Interface Sci., vol. 131, p. 514 (1989)
14 *Meyyappan, M., Subramanian, R. S.*: Thermocapillary Migration of a Gas Bubble In an Arbitrary Direction With Respect to a Plane Surface. J. Colloid Interface Sci., vol. 115(1), p. 206 (1987)
15 *Meyyappan, M., Subramanian, R. S.*: The Thermocapillary Motion of Two Bubbles Oriented Arbitrarily Relative to a Thermal Gradient. J. Colloid Interface Sci., vol. 97(1), p. 291 (1984)
16 *Meyyappan, M., Wilcox, W. R., Subramanian, R. S.*: The Slow Axisymmetric Motion of Two Bubbles in a Thermal Gradient. J. Colloid Interface Sci., vol. 94(1), p. 243 (1983)
17 *Meyyappan, M., Wilcox, W. R., Subramanian, R. S.*: Thermocapillary Migration of a Bubble Normal to a Plane Surface. J. Colloid Interface Sci., vol. 83, p. 199 (1981)
18 *Shankar, N., Subramanian, R. S.*: The Slow Axisymmetric Thermocapillary Migration of an Eccentrically Placed Bubble Inside a Drop in Zero Gravity. J. Colloid Interface Sci., vol. 94(1), p. 258 (1983)
19 *Bauer, H. F., Eidel, W.*: Marangoni-convection in a Spherical Liquid System. Acta Astronautica, vol. 15, p. 275 (1987)
20 *Oliver, D. L. R., DeWitt, K. J.*: Surface Tension Driven Flows in a Micro-gravity Environment. Int. J. Heat Transfer, vol. 31, p. 1534 (1988)
21 *Sadhal, S. S., Ayyaswamy, P. S., Chung, J. N.*: Transport Phenomena with Drops and Bubbles. Springer-Verlag, New York (1997)
22 *Subramanian, R. S.*: The Motion of Bubbles and Drops in Reduced Gravity; in: Transport Process with Drops and Bubbles, *R. P. Chhabra, D. DeKee* (eds.) p. 1–32, Hemisphere (1982)
23 *Wozniak, G., Siekmann, J., Srulijes, J.*: Thermocapillary Bubble and Drop Dynamics Under Reduced Gravity – Survey and Prospects. Z. Flugwiss. Weltraumforsch, vol. 12, p. 137 (1988)
24 *Scholze, H.*: Glass. Nature, Structure and Properties (translated by *M. J. Lakin*). Springer-Verlag, New York (1990)
25 *Happel, J., Brenner, H.*: Low Reynolds Number Hydrodynamics. Martinus Nijhoff, The Hague (1983)

Singular Perturbation Analysis of an Acoustically Levitated Sphere: Flow About the Velocity Node

Hong Zhao & S.S. Sadhal
Department of Mechanical Engineering
University of Southern California
Los Angeles, CA 90089-1453

and

Eugene H. Trinh
Jet Propulsion Laboratory
4800 Oak Grove Drive
Pasadena, CA 91109

Abstract: This analysis consists of the development of the fluid flow about a spherical particle placed at the velocity node of a standing wave. High-frequency acoustic fields are being used to levitate particles in Earth gravity, and to stabilize particles in low-gravity situations. While a standing wave in an infinite medium may be purely oscillatory with no net flow components, the interaction with particles or solid walls leads to nonlinear efffects that create a net steady component of the flow. In the present development, the perturbation procedure of Riley [9] is employed to derive the flow field for the situation when a spherical particle is positioned at the velocity node. As in Riley's [9] solution which applies to a sphere at the velocity antinode, it is found that there is a thin shear-wave region adjacent to the spherical boundary. However, this thin Stokes layer does not cover the entire sphere as in the previous case, but lies mostly around the equatorial region of the sphere. On the remaining surface of the sphere the Stokes layer opens to the surrounding flow field.

Nomenclature

a	radius of the sphere
M^2	frequency parameter, $a^2\omega/\nu$
r	radial coordinate, r^*/a
R	Reynolds number, $U_\infty a/\nu$
R_s	streaming Reynolds number, $U_\infty^2/\omega\nu = \varepsilon^2 M^2$
t	time
U_∞	velocity amplitude in the sound wave
z	coordinate along the polar axis

Greek Letters

δ	Stokes layer thickness, $\sqrt{\nu/\omega}$
ε	perturbation parameter, $\varepsilon = U_\infty/\omega a$
η	normal boundary layer coordinate [equation (18)]
θ	angular coordinate
λ	wavelength of the sound field, viscosity ratio
$\bar{\mu}$	$\cos\theta$
ν	kinematic viscosity of the fluid
ϱ	radial cylindrical coordinate, $\varrho = r\sin\theta$
τ	dimensionless time, ωt
ψ, Ψ	dimensionless stream function
ω	angular frequency

Superscripts

$*$	represents nondimensional quantities

1 Introduction

The potential for the development of both fundamental and applied sciences in the area of liquid undercooling with containerless experiments is now well established. With the achievement of deep undercooling in zero gravity, the possibility of new materials is becoming evident. It is now well known that this high degree of undercooling can promote certain types of crystal growth and at the same type provide homogeneity of the product.

In an Earth-gravity field, some degree of undercooling can be achieved by acoustic and/or electrostatic levitation. With the application of the principle of radiation pressure, ultrasound levitators have been in use for many years in ground based experiments [1, 2, 3, 7]. The recent advances in single particle levitation technology have rekindled scientific interest in the determination of the bulk and surface physical properties of liquids in the metastable supercooled, supersaturated, or superheated states. The capability of indefinitely suspending in a host fluid or vacuum, a high-purity liquid in the form of a free drop, without inducing large scale translational or oscillatory motion has created the opportunity to accurately determine the temperature dependence of a number of its thermodynamic properties. It has also become possible to observe and to quantify the rates of transport processes involving its free surface and the surrounding fluids, and to examine the details of phase transformations such as melting and solidification, evaporation and condensation.

The acoustic field provides the radiation pressure necessary to levitate a liquid drop in a gravitational field. The studies on the effects of radiation pressure on spheres and disks goes as far back as the 1930 when some of the earliest theoretical studies were conducted by King [4, 5]. With the application of this principle, ultrasound levitators have been in use for many years in ground based experiments. Electrostatic levitation is another way for containerless processing. In zero gravity, the acoustic field can be used to stabilize a fluid particle.

Acoustic streaming can be classified as two common types. One happens because of the spatial attenuation of a wave in free space, e.g., an attenuating beam of plane traveling wave. This type of streaming is usually associated with a high Reynolds number flow. The second mechanism arises from the friction between the medium and a solid wall when the former is vibrating in contact with the latter, e.g., a wave traveling down a wave-guide, a standing wave in a resonant chamber, or a wave scattering off a solid object. Unlike the spatial attenuation mentioned earlier, this effect is largely confined to a thin viscous boundary layer of thickness $\delta = (2\nu/\omega)^{1/2}$ on the surface, where ν is the kinematic viscosity of the medium and ω is the angular frequency of the wave. It is also a significant dissipation mechanism, and provides a strong force in driving acoustic streaming. While the medium outside the layer vibrates irrotationally as in a sound field, the one within the layer has vorticity because its motion has to conform to the no slip condition on wall. We are now interested in this second mechanism of streaming.

If a body of typical dimension a oscillates with velocity, say, $U_\infty \cos(\omega t)$ in a viscous fluid and $\varepsilon = U_\infty/\omega a \ll 1$, then, although the leading order solution is oscillatory, higher

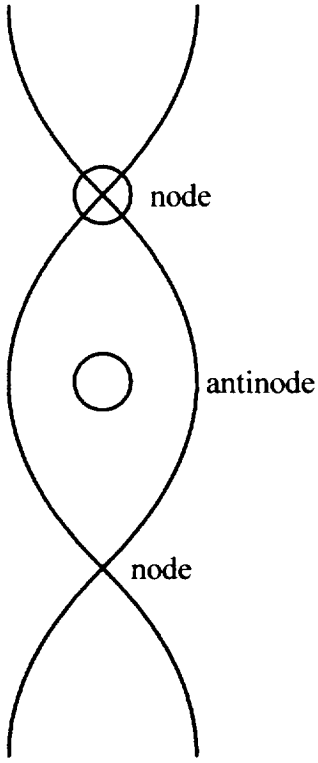

Figure 1: Velocity node and antinode identification

order terms include not only higher harmonics but steady contributions to the velocity. Mathematically, this can be explained by existence of the nonlinear terms which may have steady nonzero component. Physically, the condition $\varepsilon \ll 1$ implies that the amplitude of the oscillation is small compared with the particle radius a. The existence of this steady streaming was first pointed out by Rayleigh [8] in his work on Kundt's dust tube and was later studied in a boundary layer context by Schlichting [10] who considered flows with the additional constraint $|M|^2 = \omega a^2/\nu \gg 1$, where ν denotes the kinematic viscosity of the fluid. For such a flow it is now well established that the first order fluctuation vorticity is confined to a shear-wave region of thickness $O(\nu/\omega)^{1/2}$ beyond which steady velocities $O(\varepsilon U_\infty)$ persist. Riley [9] has considered the case of an oscillating sphere for both $|M| \gg 1$ and $0 < |M| < 1$. He calculated the streaming around the sphere which is at the velocity antinode of the wave that vibrates vertically.

In the analytical investigations to date, little consideration has been given to a particle placed at the velocity node of the wave. The velocity node and antinode are identified in Figure 1. The results from the investigation of the flow field will provide information about the characteristics of the levitation process. The theory will be very useful in overcoming some of experimental problems by providing suitable direction. For example, presently with acoustic levitation there is a residual flow field, including solid-body rotation for drops. Such instabilities interfere with, for example, the steady application of thermal stimuli which would serve as a means for the measurement of thermophysi-

cal properties. This problem needs to be solved and detailed understanding of the flow studies would be beneficial. Furthermore, very little is known about the pressure field. The flow calculations together with experimental measurements of the drop position can be used to predict the pressure field which is difficult to measure. For levitation under zero-gravity conditions, the drop assumes an equilibrium position at the velocity antinode when the external medium is a gas. When the particle phase has higher compressibility than the external phase (e.g., a gas bubble in a liquid), of if the particle is very small, the equilibrium position is at the velocity node. While the antinode solution has been available from Riley's [9] work, the node solution is a new development.

In the discussion here, the focus is on the analysis of solid sphere being placed at the velocity node of the wave. Besides the direct application to such physical cases, the analysis about the velocity node leads to an important result for calculating the streaming when the sphere is placed between the velocity node and antinode of the wave. Eventually, the analysis will be used to obtain the flow field for a sphere levitated at a position between the node and the antinode. In this proposed development, use will be made of the existing antinode solution of Riley [9] and the present node solution through a nonlinear combination. Although Lee & Wang [6] have considered this kind of problem, their result depends on an algorithm for calculating the tangential velocity on the edge of the recirculating shear layer. Detailed flow field in the shear layer for such situations are yet unavailable. A more rigorous development of the flow field is necessary to fully understand the fluid mechanics, and the present calculations provide an additional component for the complete development.

Riley [9] gave the solution for an oscillating sphere in an otherwise quiescent infinite fluid medium. This solution is applicable to to a small sphere positioned at the velocity antinode of a standing wave provided $a \ll \lambda$, i.e., the size of the sphere is small compared to the wavelength. We briefly discuss Riley's [9] solution since it forms a basis for further development. The following dimensionless parameters are relevant:

$$R = \frac{U_\infty a}{\nu} \quad M^2 = \frac{i\omega a^2}{\nu} \quad \text{and} \quad \frac{R}{|M|^2} = \varepsilon = \frac{U_\infty}{\omega a} \ll 1, \tag{1}$$

where U_∞ is a characteristic velocity and R is the Reynolds number. While Riley [9] considered both $|M| \ll 1$ and $|M| \gg 1$, the latter case (high frequency) is the one relevant to ultrasound levitation.

For a standing wave with velocity

$$u_z = U'_\infty \sin kz \, e^{i\omega t}, \tag{2}$$

the local velocity in the neighborhood of the node ($z = 0$) is

$$u_z = U'_\infty \left(kz - \frac{k^3 z^3}{3!} \cdots \right) e^{i\omega t}. \tag{3}$$

With a small particle at the antinode, the surrounding field may just be taken as the first term

$$u_z = U'_\infty kz \, e^{i\omega t} = U_\infty (z/a) e^{i\omega t}, \tag{4}$$

where $U_\infty = U'_\infty ka$.

2 Equations of Motion

By scaling the flow parameters as follows:

$$\boldsymbol{u}^* = \frac{\boldsymbol{u}}{U_\infty}, \quad \psi^* = \frac{\psi}{U_\infty a^2}, \quad \boldsymbol{x}^* = \frac{\boldsymbol{x}}{a}, \quad \text{and} \quad \tau = \omega t, \tag{5}$$

and dropping the asterisks, the Navier–Stokes equation of motion, in the stream function formulation, may be written as

$$\frac{\partial(D^2\psi)}{\partial\tau} + \frac{\varepsilon}{r^2}\left[\frac{\partial(\psi, D^2\psi)}{\partial(r,\bar{\mu})} + 2D^2\psi\, L\psi\right] = \frac{D^4\psi}{|M|^2}, \tag{6}$$

where

$$\begin{aligned} D^2 &= \frac{\partial^2}{\partial r^2} + \left(\frac{1-\bar{\mu}^2}{r^2}\right)\frac{\partial^2}{\partial\bar{\mu}^2}, \\ L &= \left(\frac{\bar{\mu}}{1-\bar{\mu}^2}\right)\frac{\partial}{\partial r} + \left(\frac{1}{r}\right)\frac{\partial}{\partial\bar{\mu}}, \end{aligned}$$

and $\bar{\mu} = \cos\theta$. The Reynolds number R, the frequency parameter M, and the perturbation parameter ε are defined in equation (1).

The stream function ψ is related to the velocity components as follows:

$$u_r = -\frac{1}{r^2}\frac{\partial\psi}{\partial\bar{\mu}} \qquad \text{and} \qquad u_\theta = -\frac{(1-\bar{\mu}^2)^{-\frac{1}{2}}}{r}\frac{\partial\psi}{\partial r}. \tag{7}$$

With this formulation the continuity condition for an incompressible fluid is satisfied. The flow may be regarded as incompressible for low Mach number.

The boundary conditions are

$$\psi = \frac{\partial\psi}{\partial r} = 0 \quad \text{on} \quad r = 1 \qquad \text{(no slip)}, \tag{8}$$

and

$$\psi \to \tfrac{1}{2}\varrho^2 z e^{i\omega t} = \tfrac{1}{2} r^3\bar{\mu}(1-\bar{\mu}^2)e^{i\tau} \quad \text{as} \quad r \to \infty, \tag{9}$$

where $\varrho = r\sin\theta$. This far-field condition is derived from the velocity field in the neighborhood of the node, given by equation (4).

3 Solution

We seek a perturbation solution in the in the outer flow region by writing

$$\psi = \psi_0 + \varepsilon\psi_1 + O(\varepsilon^2) \tag{10}$$

Similarly, in the shear-wave layer the following perturbation expansion is used:

$$\Psi = \Psi_0 + \varepsilon\Psi_1 + O(\varepsilon^2), \tag{11}$$

where Ψ is related to ψ through

$$\Psi = \frac{R_s^{\frac{1}{2}}\psi}{\varepsilon\sqrt{2}}. \tag{12}$$

Here $R_s = \varepsilon R$ is the streaming Reynolds number which is also considered to be small. This relationship (12) indicates that the appropriate scale for the stream function in the shear-wave layer is $U_\infty a(\nu/\omega)^{\frac{1}{2}}$ rather that $U_\infty a^2$.

3.1 The Leading-Order Solution

Upon inserting equation (10) into equation (6), we find that the leading order stream function for the outer flow satisfies

$$|M|^2\frac{\partial(D^2\psi_0)}{\partial\tau} = D^4\psi_0. \tag{13}$$

For $|M| \gg 1$, the vorticity, generated at the sphere, is confined to a thin 'shear-wave' layer of thickness $O(|M|^{-1})$. Outside this thin layer the flow field is irrotational and described by

$$\frac{\partial(D^2\psi_0)}{\partial\tau} = 0. \tag{14}$$

The boundary conditions are

$$\psi_0 = 0 \quad \text{on} \quad r = 1 \qquad \text{and} \qquad \psi_0 \sim \tfrac{1}{2}kar^3\bar{\mu}(1-\bar{\mu}^2)e^{i\tau}. \tag{15}$$

The solution to equation (14) with the same behavior in $\bar{\mu}$ as the far field is found to be

$$\psi_0 = \tfrac{1}{2}ka(r^3 - r^{-2})\bar{\mu}(1-\bar{\mu}^2)e^{i\tau}. \tag{16}$$

For the inner region, we substitute the expansion (11) into the Navier–Stokes equation (6) and obtain for the leading order,

$$\frac{\partial^3\Psi_0}{\partial\tau\partial\eta^2} = \frac{1}{2}\left(\frac{\partial^4\Psi_0}{\partial\eta^4}\right), \tag{17}$$

where

$$\eta = (r-1)\frac{|M|}{\sqrt{2}}. \tag{18}$$

The boundary conditions for Ψ_0 are

$$\frac{\partial \Psi_0}{\partial \eta} = \Psi_0 = 0 \quad \text{at} \quad \eta = 0. \tag{19}$$

The solution is found to be

$$\Psi_0 = c\left\{(1+i)\eta - 1 + e^{-(1+i)\eta}\right\}\bar{\mu}(1-\bar{\mu}^2)e^{i\tau}, \tag{20}$$

where c is an undetermined constant. Upon the expansion of ψ_0 about $r = 1$, and matching Ψ_0 with ψ_0 when $\eta \to \infty$, we obtain $c = \frac{5}{4}ka(1-i)$.

3.2 The First-Order Solutions $[O(\varepsilon)]$

The first order solutions are much more complex than the leading order solutions. With the substitution of the expansion given by equation (11) into the momentum equation (6), we obtain the following differential equation for Ψ_1:

$$\frac{\partial^3 \Psi_1}{\partial \tau \partial \eta^2} + \frac{\partial \Psi_0}{\partial \eta}\left(\frac{\partial^3 \Psi_0}{\partial \bar{\mu} \partial \eta^2}\right) - \frac{\partial \Psi_0}{\partial \bar{\mu}}\left(\frac{\partial^3 \Psi_0}{\partial \eta^3}\right) + \left(\frac{2\bar{\mu}}{1-\bar{\mu}^2}\right)\frac{\partial^2 \Psi_0}{\partial \eta^2}\left(\frac{\partial \Psi_0}{\partial \eta}\right) = \frac{1}{2}\left(\frac{\partial^4 \Psi_1}{\partial \eta^4}\right). \tag{21}$$

The solution to this equation may be written as a two-term eigenfunction expansion,

$$\Psi_1 = (ka)^2\left[f_1(\eta,\tau)\bar{\mu}(1-\bar{\mu}^2) + f_2(\eta,\tau)\bar{\mu}^3(1-\bar{\mu}^2)\right]. \tag{22}$$

By the substitution of (22) into (21), we find

$$\begin{aligned}\frac{1}{2}\left(\frac{\partial^4 f_1}{\partial \eta^4}\right)\bar{\mu}(1-\bar{\mu}^2) &= \frac{\partial^3 f_1}{\partial \tau \partial \eta^2}\bar{\mu}(1-\bar{\mu}^2) + \tfrac{25}{16}\left[2i\eta e^{-(1+i)\eta}e^{2i\tau} - 2i\eta e^{-(1-i)\eta}e^{-2i\tau}\right.\\ &\quad + 2i\eta e^{-(1+i)\eta} + 2e^{-(1+i)\eta}(1-e^{-(1-i)\eta}) - 2i\eta e^{-(1-i)\eta}\\ &\quad \left.+2e^{-(1-i)\eta}(1-e^{-(1+i)\eta})\right]\bar{\mu}(1-\bar{\mu}^2)\end{aligned} \tag{23}$$

and

$$\begin{aligned}\frac{1}{2}\left(\frac{\partial^4 f_2}{\partial \eta^4}\right)\bar{\mu}^3(1-\bar{\mu}^2) &= \frac{\partial^3 f_2}{\partial \tau \partial \eta^2}\bar{\mu}^3(1-\bar{\mu}^2) - \tfrac{75}{16}\left\{2i\eta e^{-(1+i)\eta}e^{2i\tau} - 2i\eta e^{-(1-i)\eta}e^{-2i\tau}\right.\\ &\quad + 2i\eta e^{-(1+i)\eta} + 2e^{-(1+i)\eta}(1-e^{-(1-i)\eta}) - 2i\eta e^{-(1-i)\eta}\\ &\quad \left.+ 2e^{-(1-i)\eta}(1-e^{-(1+i)\eta})\right\}\bar{\mu}^3(1-\bar{\mu}^2)\\ &\quad + \tfrac{25}{8}\left\{(1+i)e^{-(1+i)\eta}(1-e^{-(1+i)\eta})e^{2i\tau}\right.\\ &\quad + (1-i)e^{-(1-i)\eta}(1-e^{-(1-i)\eta})e^{-2i\tau}\\ &\quad + (1-i)e^{-(1-i)\eta}(1-e^{-(1+i)\eta})\\ &\quad \left.+ (1+i)e^{-(1+i)\eta}(1-e^{-(1-i)\eta})\right\}\bar{\mu}^3(1-\bar{\mu}^2).\end{aligned} \tag{24}$$

By separating the steady streaming from the unsteady part, we can write f_1 as

$$f_1(\eta,\tau) = \zeta_{20}(\eta) + \zeta_{22}(\eta)e^{2i\tau}. \tag{25}$$

With the insertion of (25) into (23), it is found that

$$\begin{aligned}\frac{1}{2}\left(\frac{d^4\zeta_{20}}{d\eta^4}\right) &= \tfrac{25}{8}\left[i\eta e^{-(1+i)\eta} + e^{-(1+i)\eta}(1-e^{-(1-i)\eta}) - i\eta e^{-(1-i)\eta}\right. \\ &\left. + e^{-(1-i)\eta}(1-e^{-(1+i)\eta})\right],\end{aligned} \tag{26}$$

and

$$\frac{1}{4}\left(\frac{d^4\zeta_{22}}{d\eta^4}\right) = i\frac{d^2\zeta_{22}}{d\eta^2} + \tfrac{25}{8}i\eta e^{-(1+i)\eta}, \tag{27}$$

with boundary conditions

$$\zeta_{20} = \frac{d\zeta_{20}}{d\eta} = 0 \quad \text{and} \quad \zeta_{22} = \frac{d\zeta_{22}}{d\eta} = 0 \quad \text{at} \quad \eta = 0.$$

The solution for equations (26) and (27) are found to be

$$\zeta_{20} = -\tfrac{25}{32}e^{-2\eta} - \tfrac{25}{8}\eta e^{-\eta}\sin\eta - \tfrac{75}{8}e^{-\eta}\cos\eta - \tfrac{25}{4}e^{-\eta}\sin\eta + \tfrac{325}{32} - \tfrac{75}{16}\eta \tag{28}$$

$$\zeta_{22} = \tfrac{25}{32}[\sqrt{2}(1+i)]e^{-\sqrt{2}(1+i)\eta} - \tfrac{25}{32}[\sqrt{2}(1+i)] + \tfrac{25}{8}i\eta e^{-(1+i)\eta}. \tag{29}$$

As in the case of $f_1(\eta,\tau)$, the function $f_2(\eta,\tau)$ may be decomposed in the form

$$f_2(\eta,\tau) = \zeta_{30}(\eta) + \zeta_{32}(\eta)e^{2i\tau}. \tag{30}$$

By the substitution of (30) into (24), we obtain

$$\frac{d^4\zeta_{30}}{d\eta^4} = \tfrac{25}{2}\left[-3\eta e^{-\eta}\sin\eta + 3e^{-2\eta} - 2e^{-\eta}\cos\eta + e^{-\eta}\sin\eta\right] \tag{31}$$

and

$$\frac{1}{4}\left(\frac{d^4\zeta_{32}}{d\eta^4}\right) = i\frac{d^2\zeta_{32}}{d\eta^2} - \tfrac{75}{8}i\eta e^{-(1+i)\eta} + \tfrac{25}{8}(1+i)e^{-(1+i)\eta}(1-e^{-(1+i)\eta}), \tag{32}$$

with boundary conditions

$$\zeta_{30} = \frac{d\zeta_{30}}{d\eta} = 0 \quad \text{at} \quad \eta = 0$$

and

$$\zeta_{32} = \frac{d\zeta_{32}}{d\eta} = 0 \quad \text{at} \quad \eta = 0.$$

The solutions to equations (31) and (32) are found to be

$$\zeta_{30} = \tfrac{75}{32}e^{-2\eta} + \tfrac{75}{8}\eta e^{-\eta}\sin\eta + 25e^{-\eta}\cos\eta + \tfrac{125}{8}e^{-\eta}\sin\eta - \tfrac{875}{32} + \tfrac{225}{16}\eta \quad (33)$$

$$\begin{aligned}\zeta_{32} &= \tfrac{25}{8}(1+i)e^{-(1+i)\eta} - \tfrac{75}{8}i\eta e^{-(1+i)\eta} + \frac{25}{64}(1+i)e^{-2(1+i)\eta} \\ &\quad + \tfrac{25}{64}(1+i)\left[(11\sqrt{2}-9) - 11\sqrt{2}e^{-\sqrt{2}(1+i)\eta}\right]. \end{aligned} \quad (34)$$

As a result,

$$\begin{aligned}\Psi_1 &= (ka)^2\left\{\left(-\tfrac{25}{32}e^{-2\eta} - \tfrac{25}{8}\eta e^{-\eta}\sin\eta - \tfrac{75}{8}e^{-\eta}\cos\eta - \tfrac{25}{4}e^{-\eta}\sin\eta + \tfrac{325}{32} - \tfrac{75}{16}\eta\right)\right. \\ &\quad \left. + \left[\tfrac{25}{32}(1+i)\sqrt{2}\left(e^{-\sqrt{2}(1+i)\eta} - 1\right) + \tfrac{25}{8}i\eta e^{-(1+i)\eta}\right]e^{2i\tau}\right\}\bar{\mu}(1-\bar{\mu}^2) \\ &\quad + \left\{\left(\tfrac{75}{32}e^{-2\eta} + \tfrac{75}{8}\eta e^{-\eta}\sin\eta + 25e^{-\eta}\cos\eta + \tfrac{125}{8}e^{-\eta}\sin\eta - \tfrac{875}{32} + \tfrac{225}{16}\eta\right)\right. \\ &\quad + \left[\tfrac{25}{8}(1+i)e^{-(1+i)\eta} - \tfrac{75}{8}i\eta e^{-(1+i)\eta} + \tfrac{25}{64}(1+i)e^{-2(1+i)\eta}\right. \\ &\quad \left.\left. + \tfrac{25}{64}(1+i)\left(11\sqrt{2} - 9e^{-\sqrt{2}(1+i)\eta}\right)\right]e^{2i\tau}\right\}\bar{\mu}^3(1-\bar{\mu}^2). \end{aligned} \quad (35)$$

Thus, the first order velocity has a steady part that exists outside the shear-wave layer and induces a steady streaming velocity $O(\varepsilon)$ outside that region. Upon letting $\eta \to \infty$, we see that at the edge of the shear-wave region,

$$\begin{aligned}\Psi &\sim \tfrac{5}{2}(ka)\left\{\eta\cos\tau - (\tfrac{1}{2})\sqrt{2}\cos(\tau - \tfrac{1}{4}\pi)\right\}\bar{\mu}(1-\bar{\mu}^2) \\ &\quad + \varepsilon(ka)^2\left\{(\tfrac{325}{32} - \tfrac{75}{16}\eta) - \tfrac{25}{16}\cos(2\tau + \tfrac{1}{4}\pi)\right\}\bar{\mu}(1-\bar{\mu}^2) \\ &\quad + \varepsilon(ka)^2\left\{(-\tfrac{875}{32} + \tfrac{225}{16}\eta) + \tfrac{25}{32}(11\sqrt{2}-9)\cos(2\tau + \tfrac{1}{4}\pi)\right\}\bar{\mu}^3(1-\bar{\mu}^2). \end{aligned} \quad (36)$$

Here it is clear that Ψ has the steady component

$$\begin{aligned}\Psi_s &= \varepsilon\left[\left(\tfrac{325}{32} - \tfrac{75}{16}\eta\right)\bar{\mu}(1-\bar{\mu}^2) + \left(-\tfrac{875}{32} + \tfrac{225}{16}\eta\right)\bar{\mu}^3(1-\bar{\mu}^2)\right] + O(\varepsilon^2) \\ &= \varepsilon(\tfrac{25}{32})\left[\left(13 - 35\bar{\mu}^2\right) - 6\left(1 - 3\bar{\mu}^2\right)\eta\right]\bar{\mu}(1-\bar{\mu}^2) + O(\varepsilon^2). \end{aligned} \quad (37)$$

In the outer region where $r - 1 = O(1)$, we need an asymptotic solution that should satisfy the far-field condition in equation (15), and as $r \to 1$, it should match with the inner solution as $\eta \to \infty$. Therefore, in the outer region we have equation (10) for ψ where ψ_1 satisfies the condition that as $r \to \infty$, $\psi_1 = o(r^3)$. The boundary condition in the inner region can be obtained from the matching condition and we may infer the behavior of ψ in the inner region in terms of the inner variables [equations (18) and (12)] by letting $r \to 1$ in equation (36) for Ψ. The equation for the function ψ_1 is obtained by equating coefficients of powers of ε in (6). The terms of $O(\varepsilon)$ give

$$\frac{\partial}{\partial\tau}(D^2\psi_1) = 0 \quad (38)$$

We can further write ψ_1 as

$$\psi_1 = F_1(r,\bar{\mu}) + G_1(r,\bar{\mu})\phi(\tau), \quad (39)$$

thus separating the steady streaming from the unsteady part. Upon inserting (39) into (38), we obtain the following equation for G_1:

$$D^2 G_1 = 0, \tag{40}$$

with boundary conditions

$$G_1 = o(r^3) \quad \text{as} \quad r \to \infty$$
$$G_1 \sim \bar{\mu}(1-\bar{\mu}^2) \quad \text{as} \quad r \to 1.$$

The solution of (40) for $G_1(r,\bar{\mu})$ is

$$G_1 = \frac{\bar{\mu}(1-\bar{\mu}^2)}{r^2}. \tag{41}$$

As discussed above, the matching conditions for (36) and (39) determine $\phi(\tau)$. Therefore, letting $\eta \to 0$ in equation (36) and matching $O(\varepsilon)$ terms with ψ_1, it is not difficult to see that

$$\phi(\tau) = -\tfrac{5}{2}(ka)R_s^{-\frac{1}{2}}\cos(\tau - \tfrac{1}{4}\pi).$$

Following Riley's [9] perturbation method and using some scaling arguments, $F_1(r,\bar{\mu})$ should satisfy

$$D^4 F_1(r,\bar{\mu}) = 0. \tag{42}$$

To solve (42), an intermediate function $H(r,\bar{\mu})$ is defined so that

$$D^2 F_1 = H$$

and

$$D^2 H = 0. \tag{43}$$

The solution for $H(r,\bar{\mu})$ is

$$H(r,\bar{\mu}) = \sum_{n=0}^{\infty}(A_n r^{n+1} + B_n r^{-n})C_{n+1}^{-\frac{1}{2}}(\bar{\mu}) \tag{44}$$

where

$$C_{n+1}^{-\frac{1}{2}}(\bar{\mu}) = \frac{(1-\bar{\mu}^2)}{n(1+n)}\frac{dP_n}{d\bar{\mu}} \quad for \quad n \geq 1$$

and

$$C_1^{-\frac{1}{2}}(\bar{\mu}) = -\bar{\mu}$$

in which $P_n(\bar{\mu})$ is the Legendre polynomial. The solution for $F_1(r,\bar{\mu})$ takes the form

$$F_1(r,\bar{\mu}) = \sum_{n=0}^{\infty} f_n(r)C_{n+1}^{-\frac{1}{2}}(\bar{\mu}) \tag{45}$$

where $f_n(r)$ satisfies

$$f_n''(r) + \frac{1}{r^2}(-n(n+1))f_n(r) = A_n r^{n+1} + B_n r^{-n}. \tag{46}$$

Thus the solution to equation (46) is

$$f_n(r) = C_n r^{n+1} + D_n r^{-n} + E_n r^{n+3} + F_n r^{-n+2} \tag{47}$$

where A_n, B_n, C_n, D_n, E_n and F_n are constants to be determined. The function $f_n(r)$ must satisfy the condition that $f_n(r) = o(r^2)$ as $r \to \infty$ and the inner boundary matching condition. So, $F_1(r, \bar{\mu})$ can be written as

$$\begin{aligned} F_1(r,\bar{\mu}) &= (D_2 r^{-2} + F_2)\bar{\mu}(1-\bar{\mu}^2) + (D_4 r^{-4} + F_4 r^{-2})(7\bar{\mu}^3 - 3\bar{\mu})(1-\bar{\mu}^2) \\ &= (D_2 r^{-2} + F_2 - 3D_4 r^{-4} - 3F_4 r^{-2})\bar{\mu}(1-\bar{\mu}^2) \\ &\quad + 7(D_4 r^{-4} + F_4 r^{-2})\bar{\mu}^3(1-\bar{\mu}^2). \end{aligned} \tag{48}$$

Now by letting $r \to 1$ and introducing the inner variable η defined in (18), we have

$$\begin{aligned} F_1(r,\bar{\mu}) \sim & \left\{(D_2 + F_2 - 3D_4 - 3F_4) + (-2D_2 + 12D_4 + 6F_4)\frac{\varepsilon\sqrt{2}}{R_s^{\frac{1}{2}}}\eta\right\}\bar{\mu}(1-\bar{\mu}^2) \\ & + \left\{(7D_4 + 7F_4) + (-28D_4 - 14F_4)\frac{\varepsilon\sqrt{2}}{R_s^{\frac{1}{2}}}\eta\right\}\bar{\mu}^3(1-\bar{\mu}^2) \end{aligned} \tag{49}$$

and matching to this order with (36),

$$D_2 + F_2 - 3D_4 - 3F_4 = 0 \tag{50}$$

$$-2D_2 + 12D_4 + 6F_4 = -\tfrac{75}{16} \tag{51}$$

$$7D_4 + 7F_4 = 0 \tag{52}$$

$$-28D_4 - 14F_4 = \tfrac{225}{16}. \tag{53}$$

From equations (50)–(53), we deduce that

$$D_2 = -\tfrac{75}{112}, \quad F_2 = \tfrac{75}{112}, \quad D_4 = -\tfrac{225}{224}, \quad \text{and} \quad F_4 = \tfrac{225}{224}.$$

With these constants determined, the expression for ψ_1 is found to be

$$\begin{aligned} \psi_1 = & -\tfrac{5}{2}(ka)R_s^{-\frac{1}{2}} r^{-2}\cos(\tau - \tfrac{1}{4}\pi)\bar{\mu}(1-\bar{\mu}^2) \\ & + \tfrac{75}{112}(ka)^2(1-r^{-2})\bar{\mu}(1-\bar{\mu}^2) \\ & + \tfrac{225}{224}(ka)^2(r^{-2} - r^{-4})(7\bar{\mu}^3 - 3\bar{\mu})(1-\bar{\mu}^2). \end{aligned} \tag{54}$$

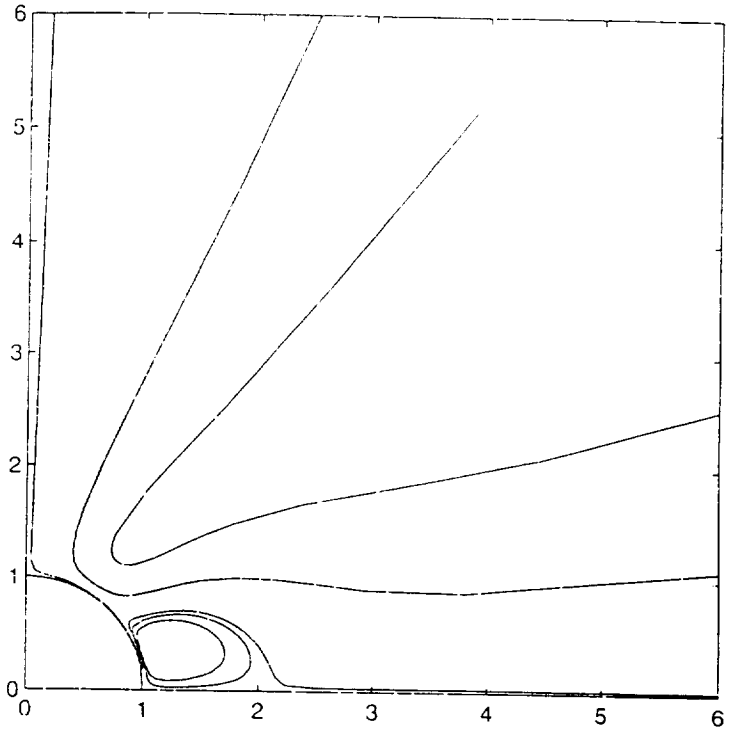

Figure 2: Steady streaming flow streamlines about a sphere at the velocity node.

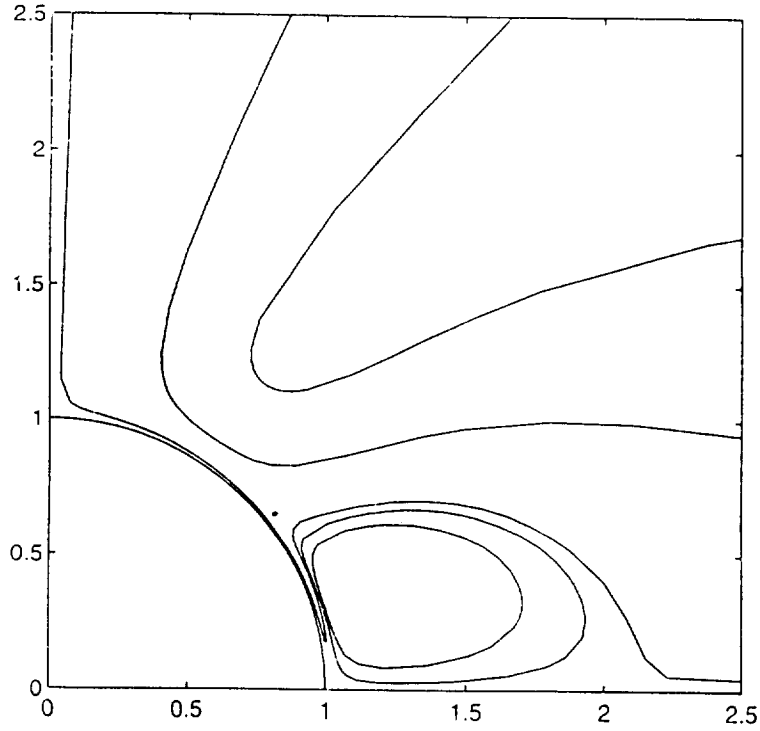

Figure 3: Detailed flow field near the sphere.

4 Discussion

The inner and outer solutions both have time-independent components which exhibit the steady streaming motion. The flow field exhibits symmetry about the polar axis and the equatorial plane. This symmetry is to be expected since the problem, as defined, is symmetric. The streamlines have been plotted for one quadrant in Figure 2. The detailed flow near the sphere is shown in Figure 3. Some interesting flow patterns have been predicted. While there is a thin layer on the surface of the particle, as in the case a particle at the velocity antinode, the streamlines are not closed. The reverse flows within the layer exist only for a belt-shaped region about the equator. Specifically, for angular positions in the range $55° < \theta < 125°$ with the polar axis, the thin layer of reverse flows is found. These values correspond to $\cos^2\theta = \frac{1}{3}$ which represents the asymptotes of the stream function given by equation (37). Outside this range, around the polar regions, the streamlines merge with the exterior flow. Mathematically, this behavior results because the Stokes-layer solution consists of two components corresponding to the first and the third spherical harmonics. These solutions add up with two guaranteed zeros in the radial direction only for a limited region over the sphere as discussed.

These results have some important implications for experimental studies relating to particle levitation.

If we consider a sphere displaced from the antinode or the node of a standing wave, we need to expand the standing wave velocity u_z such that

$$u_z = A\cos[k(z+Z_0)]e^{i\tau} = [A\cos kZ_0 + A(kz)\sin kZ_0 + O(k^2z^2]e^{i\tau} \qquad (55)$$

for small ka, in which Z_0 is the displacement of the sphere from the antinode, and $k = \omega/c$. Here, the first term of equation (55) is just the far-field velocity for Riley's [9] problem, and the second term is the far-field velocity for the problem we have just discussed. That means the problem which the sphere is displaced from the antinode is the combination of the two problems we just discussed, together with some additional nonlinear terms. This is presently under investigation.

References

[1] R.E. Apfel. Technique for measuring the adiabatic compressibility, density, and sound speed of submicroliter liquid samples. *J. Acoust. Soc. America*, **59**:339–343, 1976.

[2] A. Eller. Force on a bubble in a standing acoustic wave. *J. Acoust. Soc. America.* **43**:170–171, 1968.

[3] A.R. Hanson, E.G. Domich, & H.S. Adams. Acoustic liquid droplet holder. *Rev. Sci. Instrum.*, **35**:1031–1034, 1964.

[4] L.V. King. On the acoustic radiation pressure on spheres. *Proc. Roy. Soc. London*, **147**:212–240, 1934.

[5] L.V. King. On the theory of the inertia and diffraction corrections for the Rayleigh disc. *Proc. Roy. Soc. London A*, **153**:17–40, 1935.

[6] C.P. Lee & T.G. Wang. Outer acoustic streaming. *J. Acous. Soc. America*, **88**:2367–2375, 1990.

[7] P.L. Marston & R.E. Apfel. Acoustically forced shape oscillations of hydrocarbon drops levitated in water. *J. Colloid Interface Sci.*, **68**:280–286, 1979.

[8] R.S. Rayleigh. *Phil. Trans. Roy. Soc. London A*, **245**:535–, 1883.

[9] N. Riley. On a sphere oscillating in a viscous fluid. *Quart. J. Mech. Appl. Math.*, **19**:461–472, 1966.

[10] H. Sclichting. Berechnung ebener periodischer Grenzschichtströmungen. *Physik Zeitschr.*, **XXXIII**:327–335, 1932.

Heat Transfer 1994

Proceedings of
The Tenth International
Heat Transfer Conference

Brighton, UK

Volume
5

Pool boiling
Particulates, porous media and special applications
Natural and mixed convection

Edited by
G.F. Hewitt

in cooperation with the members of the International Scientific Committee:

M. Combarnous, M. Cumo, E. Hahne, G. Hetsroni, C.J. Hoogendoorn, J.R. Howell, A.I. Leontiev, J.S. Lee, L.F. Milanez, P. Oosthuizen, V.M.K. Sastri, K. Suzuki, B.X. Wang

HTD-Vol. 332

Proceedings of the

ASME HEAT TRANSFER DIVISION

VOLUME 1

- HEAT TRANSFER IN MICROGRAVITY SYSTEMS
- RADIATIVE HEAT TRANSFER AND RADIATIVE HEAT TRANSFER IN LOW-TEMPERATURE ENVIRONMENTS
- THERMAL CONTACT CONDUCTANCE AND INVERSE PROBLEMS IN HEAT TRANSFER

presented at

THE 1996 INTERNATIONAL MECHANICAL ENGINEERING CONGRESS AND EXPOSITION
NOVEMBER 17–22, 1996
ATLANTA, GEORGIA

sponsored by

THE HEAT TRANSFER DIVISION, ASME

edited by

ASHOK GOPINATH
NAVAL POSTGRADUATE SCHOOL

S. S. SADHAL
UNIVERSITY OF SOUTHERN CALIFORNIA

PETER D. JONES
AUBURN UNIVERSITY

J. SEYED-YAGOOBI
TEXAS A&M UNIVERSITY

KEITH A. WOODBURY
THE UNIVERSITY OF ALABAMA

THE AMERICAN SOCIETY OF MECHANICAL ENGINEERS
United Engineering Center / 345 East 47th Street / New York, N.Y. 10017

HEAT TRANSFER IN MICROGRAVITY SYSTEMS

Introduction

Ashok Gopinath
Naval Postgraduate School
Monterey, California

S. S. Sadhal
University of Southern California
Los Angeles, California

Thermal phenomena in reduced gravity have attracted considerable scientific interest in a wide variety of topics including thermocapillary flows, crystal growth behavior, multiphase phenomena, containerless processing of drops and bubbles, and combustion, to name a few. This exciting branch of fluid mechanics and heat transfer offers a lot of promise for future scientific development, particularly in the creation of new types of material. The contributions from the heat transfer community have become an important element in this development.

This symposium is part of a continuing series on Heat Transfer in Microgravity Systems sponsored by the K-6 Committee (on Energy Systems) of the ASME Heat Transfer Division. The heat transfer community involved in microgravity research has been responding with considerable enthusiasm to our call for papers over the last few years. Ten papers were presented in two sessions — one primarily on phase-change phenomena, and the other mainly on thermocapillary flows and surface effects — at the 1996 ASME International Mechanical Engineering Congress and Exposition (Atlanta, Georgia, November 17–22, 1996).

We are grateful to the authors who have participated in these sessions and offered their scientific contributions. We also thank the reviewers whose critical evaluations provided the necessary input for maintaining the technical quality of these symposia.

HTD-Vol. 235

HEAT TRANSFER IN MICROGRAVITY SYSTEMS
— 1993 —

presented at
THE 29TH NATIONAL HEAT TRANSFER CONFERENCE
ATLANTA, GEORGIA
AUGUST 8–11, 1993

sponsored by
THE HEAT TRANSFER DIVISION, ASME

edited by
S. S. SADHAL
UNIVERSITY OF SOUTHERN CALIFORNIA

A. HASHEMI
LOCKHEED PALO ALTO

THE AMERICAN SOCIETY OF MECHANICAL ENGINEERS
345 East 47th Street □ United Engineering Center □ New York, N.Y. 10017

FOREWORD

The availability of microgravity conditions has made possible certain thermal phenomena that were otherwise difficult to achieve. Among them is the deep undercooling of liquids, a state that is favorable for certain types of crystal growth. Such states may also be achieved by acoustic or electrostatic levitation, and studies involving containerless processing of materials are often associated with microgravity studies. Low gravity also allows the isolation of various thermal phenomena that would otherwise be obscured by gravity driven flows. In particular, thermocapillary flows are a popular subject of investigation in this regard. Microgravity related research is currently active in a wide variety of analytical and experimental problems dealing with levitated drops and bubbles, thermocapillary flows, low gravity combustion, crystal growth, containerless processing, and thermophysical properties of undercooled liquids.

This symposium volume consists of seven papers that were presented in two sessions. They cover several of the above topics, with participants from universities as well as government laboratories. We are thankful to all of the authors who have contributed to these sessions. We are also very grateful to the referees whose input has helped maintain the quality of ASME publications.

S. S. Sadhal
University of Southern California
Los Angeles, California

A. Hashemi
Lockheed Palo Alto
Palo Alto, California

HEAT TRANSFER IN MICROGRAVITY SYSTEMS 1994

1994 International Mechanical Engineering Congress

November

sponsored by
The Heat Transfer Division, ASME

edited by
S. S. Sadhal
University of Southern

Naval Postgraduate

THE AMERICAN SOCIETY OF MECHANICAL ENGINEERS
UNITED ENGINEERING CENTER / 345 EAST 47TH STREET

FOREWORD

Thermal phenomena in reduced gravity have attracted considerable scientific interest, particularly in deep undercooling and crystal growth. The availability of sustained microgravity conditions has made possible thermal phenomena that were otherwise difficult to achieve. In addition, low gravity experimentation has allowed the observation of certain thermal phenomena that have been obscured by the interference of gravity-dominated processes. Among them is the subject of thermocapillary flows. Much of the work on undercooling has been possible with containerless processing; this has also been achieved by acoustic or electrostatic levitation. Such ground based studies on containerless processing of materials are often placed in the realm of microgravity. Research activities related to microgravity presently cover various experimental and theoretical areas dealing with levitated drops and bubbles, containerless processing, thermophysical properties of undercooled liquids, thermocapillary flows, low gravity combustion, and crystal growth.

This is the second in a series of symposia on microgravity sponsored by the K-6 Committee (Energy Systems) of the ASME Heat Transfer Division. Ten papers are presented in two sessions – one on general papers, the second on thermocapillary flows – at the 1994 International Mechanical Engineering Congress and Exposition (Chicago, Illinois, November 6–11, 1994).

We are grateful to the authors who have participated in these sessions and offered their scientific contributions. We also thank the reviewers whose critical evaluations provided the necessary input for maintaining the technical quality of these symposia.

S. S. Sadhal
University of Southern California

A. Gopinath
Naval Postgraduate School

HTD-Vol. 305

Proceedings of the 30th

1995 NATIONAL HEAT TRANSFER CONFERENCE

VOLUME 3

- HEAT TRANSFER IN MICROGRAVITY SYSTEMS
- FUNDAMENTALS OF THREE-DIMENSIONAL NATURAL CONVECTION
- MICROCHANNEL HEAT TRANSFER

presented at

THE 1995 NATIONAL HEAT TRANSFER CONFERENCE
PORTLAND, OREGON
AUGUST 6–8, 1995

sponsored by

THE HEAT TRANSFER DIVISION, ASME

edited by

S. S. SADHAL
UNIVERSITY OF SOUTHERN CALIFORNIA

A. GOPINATH
NAVAL POSTGRADUATE SCHOOL

PATRICK H. OOSTHUIZEN
QUEENS UNIVERSITY

AB HASHEMI
LOCKHEED MARTIN

THE AMERICAN SOCIETY OF MECHANICAL ENGINEERS
United Engineering Center • 345 East 47th Street • New York N.Y. 10017

HEAT TRANSFER IN MICROGRAVITY SYSTEMS

Introduction

A. Gopinath
Naval Postgraduate School
Monterey, California

S. S. Sadhal
University of Southern California
Los Angeles, California

Low gravity research in heat transfer and fluid mechanics has always been of direct interest in space technology where the conditions necessitate the investigations of physical phenomena relevant to areas such as electronics cooling and combustion. More recently, there has been considerable scientific interest in relation to deep undercooling and crystal growth. With the availability of sustained microgravity conditions, it has become possible to create certain thermal phenomena that were otherwise difficult to achieve. Among them is the formation of new types of crystals through deep undercooling in containerless systems. Also, experimentation under low gravity has allowed the observation of thermophysical phenomena, such as thermocapillary flows, that are normally obscured by gravity-dominated processes. Research activities related to microgravity are currently covering various experimental and theoretical areas dealing with levitated drops and bubbles, containerless processing, thermophysical properties of undercooled liquids, boiling phenomena, low gravity combustion, thermocapillary flows, and crystal growth.

This symposium on microgravity is the third in a series sponsored by the K-6 Committee on Energy Systems of the ASME Heat Transfer Division. Eleven papers have been accepted for publication, and these are being presented in two sessions. The first session consists of six papers on boiling phenomena in low gravity, including a review paper. In the second session there are three papers on other topics related to microgravity heat transfer.

We appreciate the authors' participation through their scientific contributions to these sessions. At the same time, we are also grateful to the referees for providing critical reviews in order to maintain the technical quality of these contributions.

HTD-Vol. 290, Heat Transfer in Microgravity Systems
ASME 1994

ACOUSTIC STREAMING AND ULTRASONIC PROCESSING OF LOW MELTING POINT MATERIALS

E. H. Trinh and S. S. Sadhal
Jet Propulsion Laboratory
California Institute of Technology
Pasadena, California
and
University of Southern California
Los Angeles, California

ABSTRACT

Ultrasonic levitation allows the processing of low melting materials both in 1 G as well as in microgravity. The free suspension of the melts also facilitates undercooling, permitting the measurement of the physical properties of the metastable liquids. A convenient method to melt a levitated sample involves its spot heating through a focused radiant source, the heat input to the sample is controlled by the material emittance as well as the external convective flows. Because of high intensity sound fields required for levitation, thermoacoustic streaming will significantly increase the heat transfer from the sample to the environment, and it will therefore decrease the heating efficiency. Experimental measurement involving flow visualization and power input monitoring have allowed the quantitative assessment of this enhancement in heat transfer at ultrasonic frequencies and for millimeter-size samples. A decrease of temperature by up to 150 C for a sample initially at 550 C without the sound has been measured. Other results involving normal 1 G and low gravity flow visualization and material processing are presented.

INTRODUCTION

A low gravity environment is ideally suited for experimental studies involving the melting and solidification of materials in the absence of a container. The drastic reduction in the effects of the Earth gravitational acceleration allows the use of much lower levels in the electromagnetic (Okress et al., 1952, and Cummings and Blackburn, 1991), electrostatic (Rhim et al., 1993), or acoustic (Trinh, 1985) fields used to remotely position the sample of interest. Depending upon the material properties, the composition of the processing medium, and the levitation technique, the reduction of gravity could allow the study of phenomena not ordinarily observed, or it could lead to more accurate experimental measurements. For example, the decrease in the magnitude of the electromagnetic field required for positioning a molten metal droplet in low gravity could result in the enhanced supercooling of the liquid sample. The reduction of the acoustic intensity used for sample levitation in a gaseous host medium also means a reduced level of acoustically induced convective flow around the levitated sample. The effects of acoustic streaming associated with ultrasonic levitation is the subject of this experimental investigation.

The specific results to be reported below have been obtained from a flow visualization study of streaming flow fields in a single-axis ultrasonic levitator operating at 25 kHz and in 1 G. A quantitative assessment of the enhanced convective heat transfer from a locally heated sample has been obtained for moderately high sample temperature, and the results are summarized. Finally, some results of the levitation processing of low-melting materials in 1 G using ultrasonic techniques are described.

I. THE EXPERIMENTAL TECHNIQUE

A standard single-axis ultrasonic levitator (Trinh, 1985) is used to levitate the liquid and solid samples to be processed in a gaseous environment and at the focus of either a Nd-Yag laser or a Xenon arc lamp. Figure 1 provides a schematic representation of the apparatus. An ultrasonic standing wave with an integer number of half-wavelengths (typically 1.5 or 3) is established between the driver and reflector, and a sample can be levitated at any

one of the pressure nodes (acoustic velocity antinodes). In addition to the second-order radiation pressure which is at the origin of the levitation force, a second order steady-state convective flow, or acoustic streaming field, is also generated. These flows are the ultrasonic equivalent of the streaming flow fields investigated by Gopinath and Mills (1993) in the same context of the application of acoustic levitation. The visualization of these flows is carried out through light scattering by smoke particles under laser sheet illumination. The resulting streamlines are imaged by a video camera and recorded on tape. The temperature of the heated samples is determined through embedded thermocouples when they are mechanically suspended, and by the use of an infrared imaging camera when they are levitated.

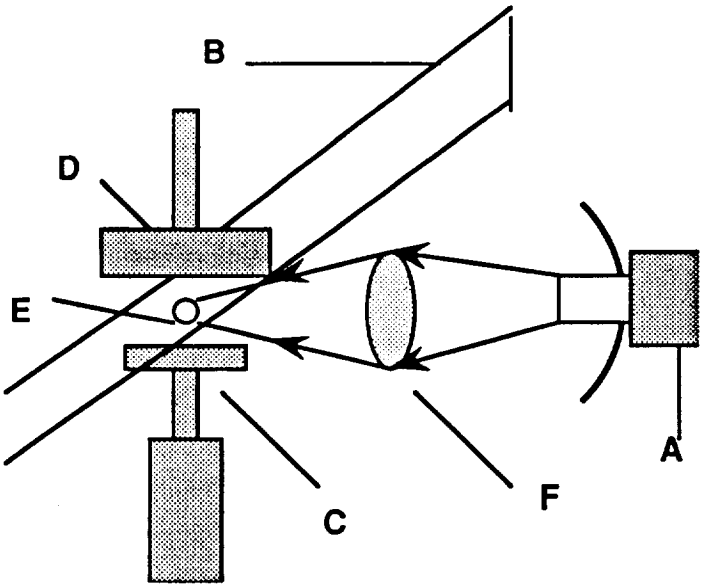

FIGURE 1

SCHEMATIC DESCRIPTION OF EXPERIMENTAL APPARATUS. THE SAMPLE (E) IS LEVITATED IN THE AXISYMMETRIC STANDING WAVE BETWEEN THE ULTRASONIC DRIVER (C) AND THE REFLECTOR (D). THE LIGHT SHEET (B) IS USED TO VISUALIZE THE FLOW FIELD THROUGH SCATTERING FROM SMOKE PARTICLES. A XENON ARC LAMP (A) BEAM IS FOCUSED ON THE SAMPLE THROUGH A LENS (F).

II. FLOW VISUALIZATION OF THERMOACOUSTIC STREAMING

Incense smoke was used as a tracer for these flow visualization studies. Previous investigations under isothermal conditions have revealed that the axial symmetry of the levitator was extended to the acoustic streaming flow field. This symmetry would not necessarily be preserved, however, in the case of a locally heated levitated or mechanically held sample because the spot heating is generally not along the axis of symmetry. With this caveat in mind, we have carried out flow visualization using sheet lighting parallel to the levitator axis of symmetry which is vertically oriented parallel to the gravity axis. The heated sample was simulated by a cylindrical mechanically held thermistor (1.9 mm diameter and 6.35 mm long). The temperature of the thermistor was varied by changing its drive voltage; its resistance was monitored by measuring the current input. All experiments were carried out at an ambient room temperature of about 23 C. The ultrasonic frequency was 25 kHz and the maximum Sound Pressure Level or SPL was 155 dB. The SPL is defined as a logarithmic relative pressure measurement with a fixed reference p_{ref} = 0.0002 μBar expressed in dB.

Figure 2 is a photograph of a video frame showing the flow pattern around the unheated cylindrical thermistor with ultrasound at 145 dB. The sound driver and the reflector (separated by 1.5 acoustic half-wavelengths) can be seen at the bottom and top of the picture together with the primary and secondary eddies. An enclosure (6.35 x 6.35 x 3.81 cm) has been placed around the levitation region in order to slow smoke dissipation. This enclosure does not significantly contribute to the primary standing wave in the region of interest around the sample. The primary set of eddies would be present in the chamber even without the thermistor, while the secondary eddies are attached to the thermistor and are caused by its presence. The primary eddy flow direction is counter-clockwise on the right side and clockwise on the left side of the picture; the direction of flow in the secondary eddies is directly opposite. Theory predicts a symmetrical set of vortices above and below the cylinder for streaming around a cylindrically shaped body. In practice, the superposition of the primary streaming flows caused by the enclosure reinforces the upper set of eddies, but opposes the lower vortices.

Figure 3 shows a still video frame for a thermistor heated to 150 C in an ultrasonic standing wave with the SPL at 140 dB. In addition to the secondary vortices attached to the upper part of the thermistor, another set of vortices reappear on the lower side of the thermistor. This reappearance of the lower vortices is probably due to natural convective flows associated with the temperature gradient caused by the hot sample immersed in a cooler gas environment.

Figure 4 shows the streaming flow field immediately around the thermistor for a temperature of 450 C and the SPL at 145 dB. The upper eddies are no longer prominent, but the lower eddies are sharper and detached from the sample. These lower eddies are also split into two sets of counter-rotating vortices. The outer component of this

pair periodically stretches outward, sheds, and reforms closer to the inner component. The frequency of vortex shedding is controlled by the tuning of the ultrasonic standing wave. For a given sample temperature, a steady flow pattern can be established and maintained if careful tuning of the ultrasound is implemented. The influence of natural convection manifests itself through the shift in the location of the attached secondary vortices: free convection induces a flow opposite to the original primary streaming flow of the isothermal chamber and reinforces the lower set of secondary vortices while washing out the upper pair.

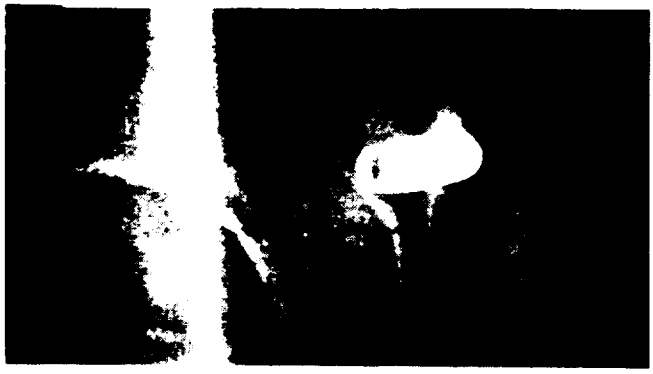

FIGURE 2
FLOW PATTERN AROUND THE UNHEATED CYLINDRICAL THERMISTOR WITH AN ULTRASONIC WAVE AT 145 dB.

FIGURE 3
FLOW PATTERN AROUND THE THERMISTOR HEATED TO 150 C WITH SOUND AT 145 dB.

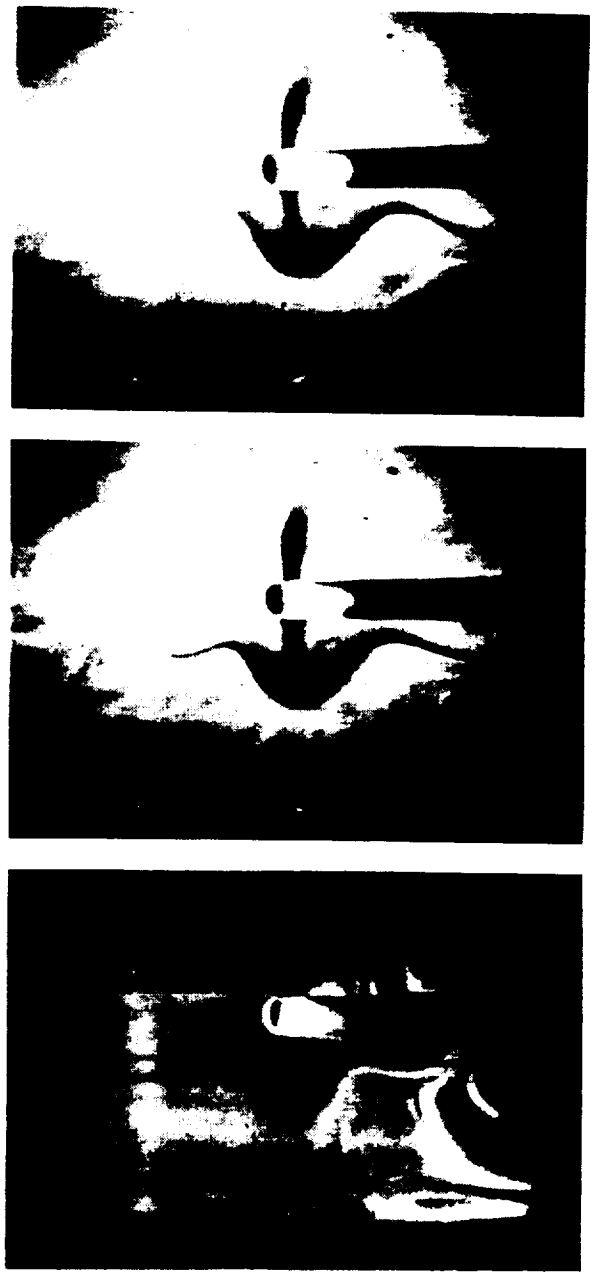

FIGURE 4
FLOW PATTERN WITH THERMISTOR AT 450 C AND SOUND AT 145 dB

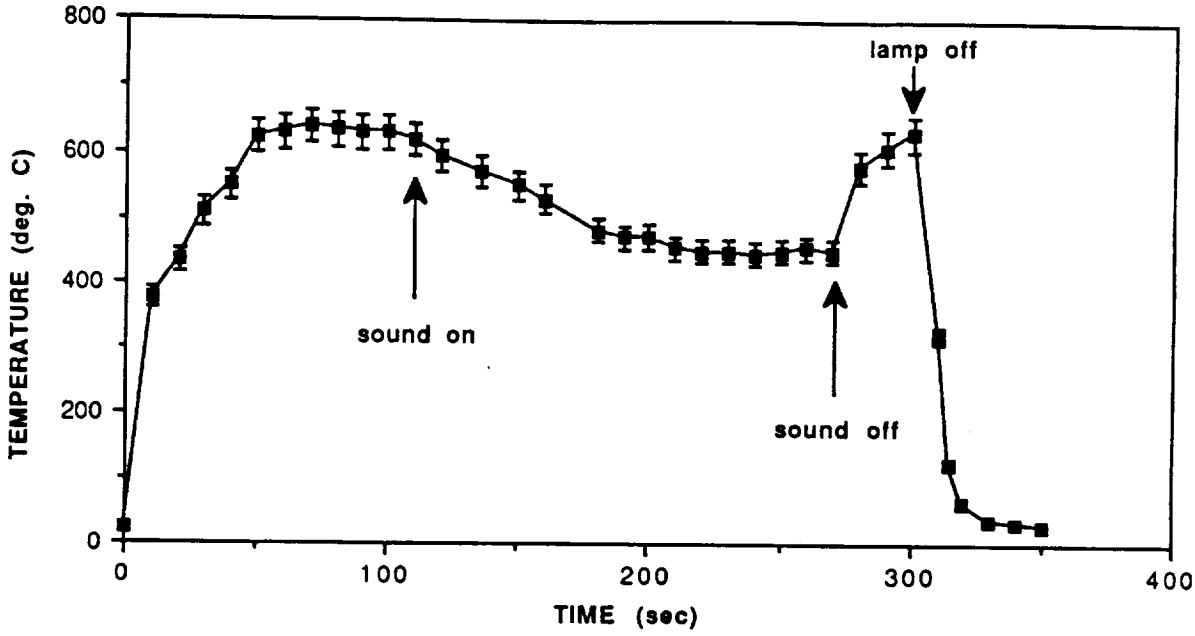

FIGURE 5
TEMPERATURE OF A SPOT-HEATED CERAMIC SAMPLE WITH AND WITHOUT THE ULTRASOUND AT 160 dB

III. THE EFFECT OF STREAMING ON FORCED CONVECTIVE HEAT TRANSFER

Figure 5 displays the results of the measurement of a spot-heated ceramic sample mechanically held at the pressure node (velocity antinode) of an ultrasonic standing wave at 160 dB. The sample was heated by focusing the light from a Xenon arc lamp on one side of the sample. The temperature was obtained from a thermocouple embedded in the spherical sample of 3 mm diameter. A dramatic drop in the sample temperature from 640 to 440 C (45% decrease) illustrates the effectiveness of forced cooling by ultrasonic streaming. Figure 6 shows that the effect of acoustic streaming is relatively large in the lower relative intensity range. Increasing the acoustic drive appears to indicate a "saturation" effect, as shown by the relatively smaller temperature drop at higher acoustic drive voltages.

In order to simulate the microgravity conditions, additional measurements were carried out using the mechanically held thermistor and relatively low SPL (145 dB). At 25 kHz and 145 dB in air at 25 C the Stokes boundary layer thickness δ ($\delta=(2\nu/\omega)^{0.5}$, where ν is the kinematic viscosity of the fluid, and ω is the angular frequency of the acoustic wave) is approximately equal to 14 μm and the acoustic displacement ($a = 2\pi U_{ac}/\omega$) is about 35 μm. U_{ac} is the acoustic particle velocity. Defining a streaming Reynolds number in the same manner as Gopinath and Mills (1993) and Leung et al. (1989): $R_s = (a / \delta)^2$, we find that the value for R_s is approximately equal to 4 for our measurements at 143.5 dB in air for a thermistor heated to 420 C.

Assuming that the thermistor is isothermal, an average Nusselt number can be calculated. $Nu = hd / \kappa$, where h is the average heat transfer coefficient, d is the thermistor diameter, and κ is the thermal conductivity of air. The average heat transfer coefficient is based on a cylindrical geometry, and can be expressed as $h = Q / A_c (\Delta T)$, where Q is the power input, A_c is the surface area of the cylinder, and ΔT is the temperature difference between the thermistor and the ambient air. The results are listed in table I for four different temperature differences between 57 and 397 C. Although the analysis of Gopinath and Mills is based on a spherical geometry, for small temperature differences, and for much larger values of R_s, the ratio $Nu / (R_s)^{0.5}$ was calculated for comparison.

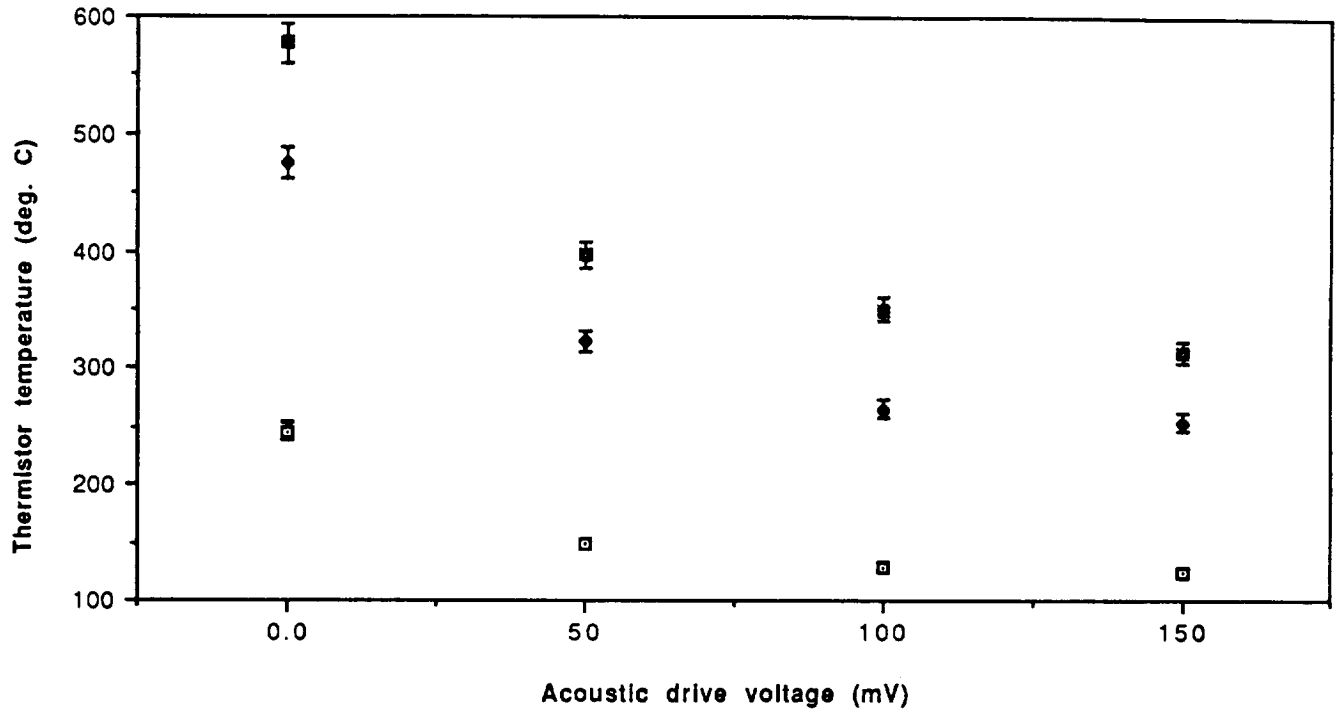

FIGURE 6

THERMISTOR TEMPERATURE AS A FUNCTION OF ACOUSTIC DRIVE FOR DIFFERENT INITIAL TEMPERATURES

$\Delta T(^{\circ}C)$	$h(W/m^2K)$	$Nu=hd/\kappa$	$Nu/(R_s)^{0.5}$
57	63	4.13	1.99
132	125.6	7.02	3.46
307	155.6	6.70	3.74
397	165.4	6.41	3.75

TABLE I

RESULTS OF THE CALCULATION OF THE AVERAGE HEAT TRANSFER COEFFICIENT AND THE AVERAGE NUSSELT NUMBER FOR FOUR DIFFERENT TEMPERATURES.

IV. DISCUSSION

Previous experimental studies of thermoacoustic streaming have also included flow visualization and heat transfer coefficient measurement (Fand and Kaye, 1961, and Fand, 1962). Most of these results were obtained for a horizontally directed *traveling* sound wave normal to the axis of the cylinder and for a ratio of the acoustic half-wavelength to the cylinder diameter which is at least equal to 6 ($\lambda/2d$ is equal to 3 in this present work). The ratio of the acoustic particle displacement to the diameter of the cylinder a/d was equal to 0.016 in the previous work while it ranges from 0.019 to 0.028 in the current investigation. In addition the previous flow visualization results were obtained with flowing smoke streams while the present ones have been based on initially stationary smoke particles. The previous studies could not therefore reveal the superposition of isothermal streaming with the thermal component. These differences explain why the current measurement of the average heat transfer coefficient for acoustically forced convective cooling yield

results which are a factor of 5 larger than the values obtained in the earlier studies.

The current flow visualization results suggest that natural convection plays a significant role in the determination of the morphology of the flow field: the resulting flow configuration is a superposition of the isothermal streaming field, natural convective flow, and the streaming flow associated with the sample itself. The principal controlling parameters are the temperature difference ΔT and the acoustic particle displacement amplitude relative to the sample diameter a/d. For moderate temperature differences ($\Delta T < 500$ C), two distinct flow field regimes appear to dominate near the sample: a symmetric pattern of four eddies both above and below the sample at lower sound intensities (SPL < 145 dB) and an asymmetric distribution where two sets of counter-rotating eddies are found at the lower half of the sample. Vortex shedding can happen, and it is probably related to the stability of the standing ultrasonic wave under thermal fluctuations. Careful tuning of the acoustic wave always appears to stabilize any large scale oscillation of the flow field. One must keep in mind that the quasi-isothermal streaming flow field characteristic of the chamber provides a background which must be taken into account in the detailed analysis of the overall fluid flow distribution. At very high sound levels (SPL > 150 dB) the smoke particle visualization technique is no longer effective because of the high velocities attained, and no clear structure can be resolved. It seems, however, that the lower vortex pattern attached to the sample still remains, even in the midst of what would appear to be turbulent flow.

V. SAMPLE PROCESSING EXPERIMENTS

Ultrasonic levitation melting, undercooling, and solidification in a gaseous environment of low melting metals, and organic or inorganic materials have been carried out in ground-based laboratories in isothermally heated chambers [9] . Spot heating of levitated samples is more difficult, however, because of the local thermal disturbance affecting an essentially rather well tuned system. The non-trivial task of maintaining levitation under the influence of acoustic streaming has been investigated in 1 G, and it can be accomplished for a sample-environment temperature difference of about 500 C for low density materials. This implies that the microgravity implementation of such a capability has been verified. The extension to higher temperature processing could be accomplished through the combination of a high temperature isothermal facility coupled to a spot heating capability.

The spot heating of materials for containerless processing is advantageous in terms of high heating and cooling rates, but it presents the disadvantage of requiring the implementation of reliable remote temperature measurement capabilities. In addition to standard single and multi-color pyrometers, we have chosen to implement infra-red imaging cameras for high temperature Earth-based developmental studies as well as for experiments in material processing.

Figure 7 reproduces video displays of an infra-red imaging camera recorded during the levitation melting of a spherical polymer sample in 1 G. The sample starts to soften and increases in volume due to boiling of volatile components. It ultimately distorts and solidifies into a non spherical sample.

Because of the thermal input from the spot heating, the ultrasonic standing wave undergoes oscillations which cause sample translational vibrations. These positional instabilities (also accompanied by rotational motion) in turn initiate thermal fluctuations because the sample has a time-dependent motion into and out of the heating beam or focal region. Earth-based processing is more sensitive to this instability process because of the high sound pressure levels required for levitation. The practical solution to this problem involves real-time, fast response ultrasound retuning as well as slow increases in the heat input. A closed-loop feedback system coupling the sound tuning and intensity to the sample motion and heat input is required for Earth-based controlled processing. The sample behavior in microgravity should remain qualitatively similar except for slower position fluctuations due to the smaller magnitude restoring force. The same active control capabilities for the levitator and heat input, however, will still be required.

Figure 8 are video still frames of the IR imager output for the Earth-based levitation heating of a low density shuttle tile sample (3 mm in diameter). The series of photographs shows the typical fluctuations in position of the sample. The maximum temperature recorded is approximately 520 to 550 C. A substantial thermal gradient exists on the surface of the sample as it is heated from one direction by a 2 mm diameter gaussian beam from a Nd-YAG CW laser.

Figure 9 shows a video still frame sequence describing the various stages of melting and solidification of an O-Terphenyl sample in low gravity during the parabolic flight of the NASA KC-135 airplane. About 15 seconds are available at an acceleration level of about 0.05 G for positioning, melting, and solidifying the sample. The resulting oblate shape is caused by the higher intensity sound required for levitation under 1.8 G during the high G part of the parabolic flight.

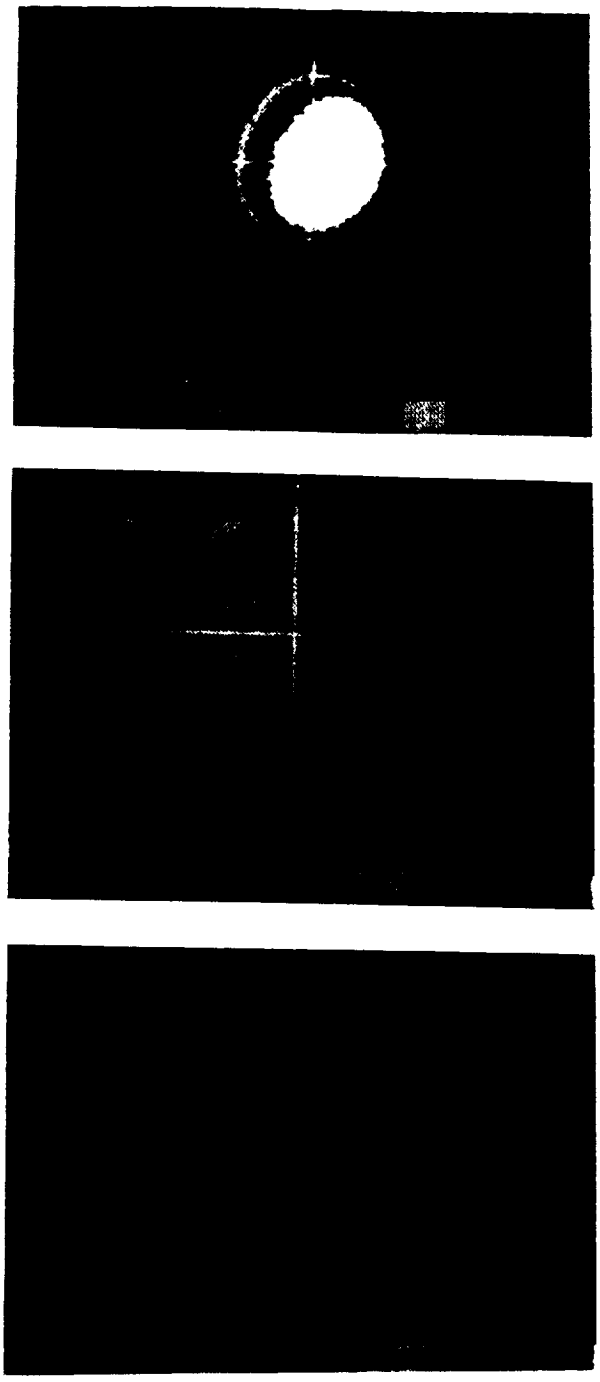

FIGURE 7

LEVITATION PROCESSING OF A SPHERICAL POLYMERIC SAMPLE IN AN ULTRASONIC FACILITY WITH FOCUSED XENON ARC LAMP HEATING

VI. SUMMARY

These preliminary experiments have provided strong evidence for the significant role played by acoustic streaming in the levitation processing of materials. Flow visualization has shown that the resulting convective field is a combination of forced isothermal streaming characteristic of the chamber, near sample boundary streaming, and finally natural buoyancy flows. The reduction of the gravitational component thus significantly alters the flow morphology by virtually eliminating the natural buoyancy component and by reducing the maximum acoustic field intensity required for sample positioning.

Results of the measurements carried out in this work also suggest that the enhancement of heat transfer quickly increases for sound pressure levels up to 150 dB, but levels out at the very high SPL. Since the lower end of the sound intensity scale is likely to be implemented in low gravity, the effect of thermo-acoustic streaming should remain an important factor in microgravity processing of materials in gases. Acoustic streaming affects not only the efficiency of spot heating of freely suspended samples, but it also significantly degrades their position and rotational stability within the ultrasonic field. An appropriately designed feedback system tying the sound tuning and intensity and heat input controls to sample position information will be required for both ground-based and microgravity processing.

Earth-based processing of low-melting polymeric and metallic materials has provided early evidence of the feasibility of spot heating for moderate sample-environment temperature difference. An experimentally determined upper limit of about 500 C for the sample-environment temperature difference has been obtained for ground-based processing of low temperature samples. The environment temperature can of course by as high as required as long as isothermal conditions are maintained and the positioning (levitation) system remains effective.

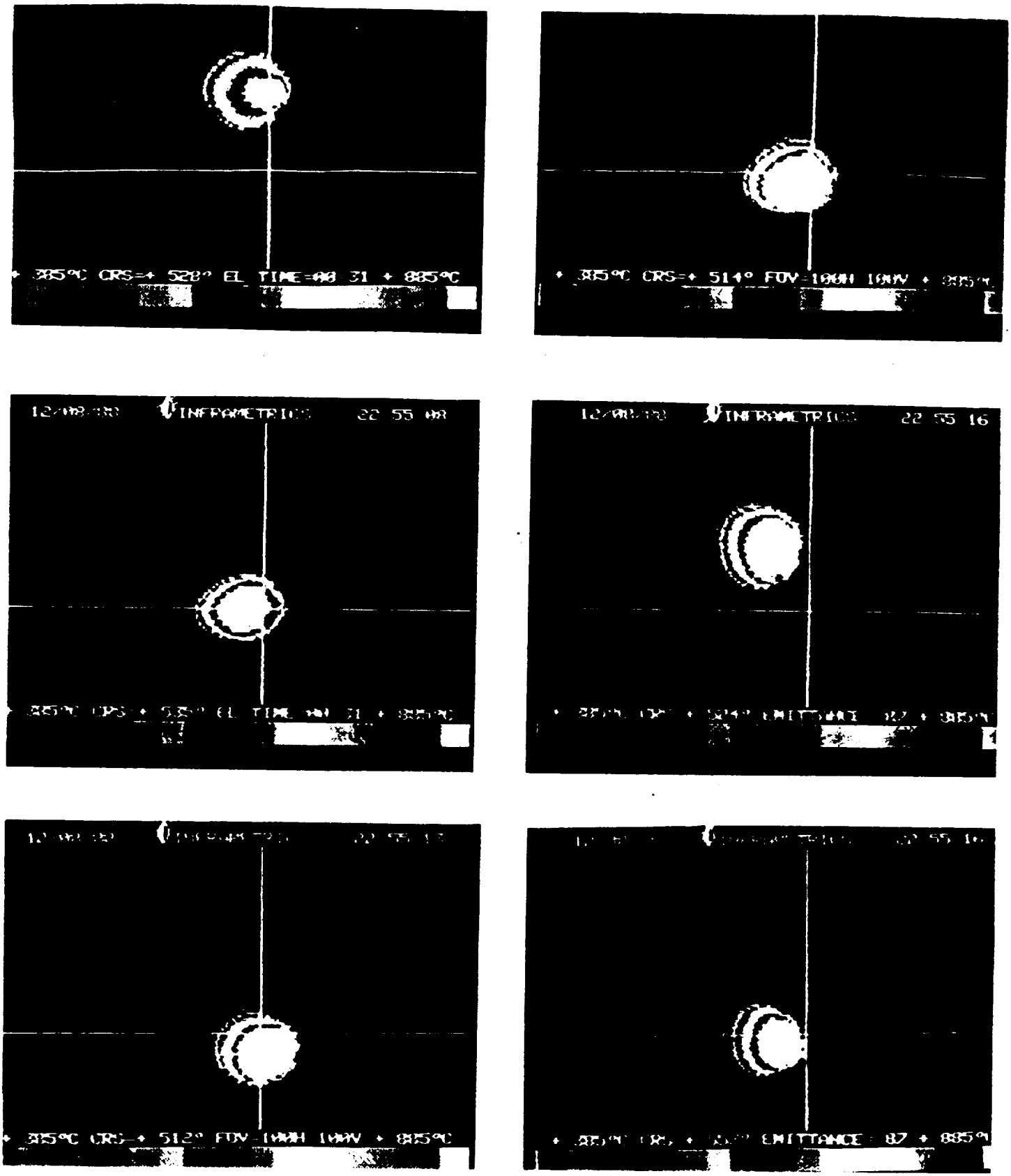

FIGURE 8
IR IMAGER OUTPUT DURING THE SPOT HEATING OF A LEVITATED SHUTTLE TILE SAMPLE IN 1 G.

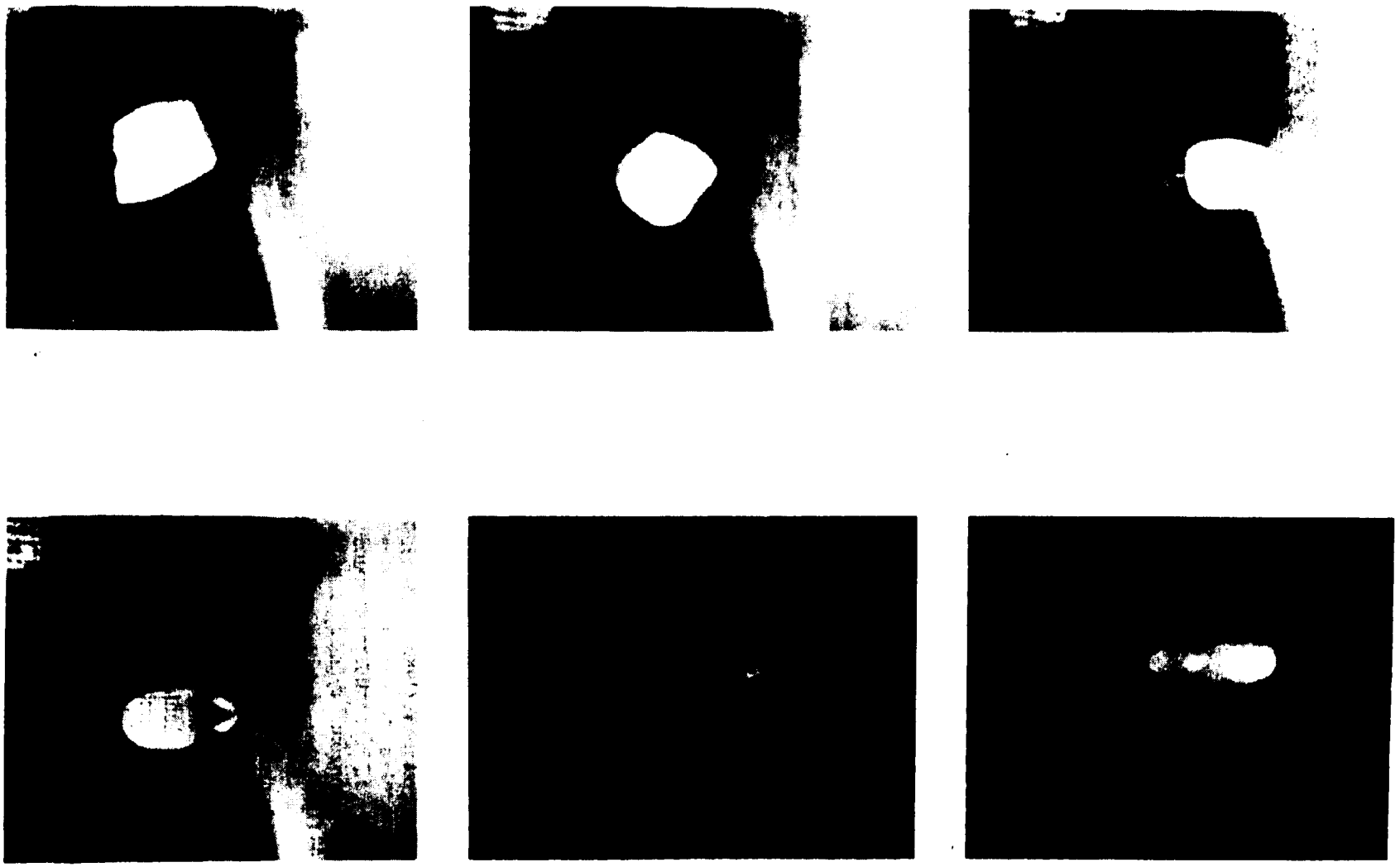

FIGURE 9

LOW GRAVITY MELTING AND SOLIDIFICATION OF O-TERPHENYL DURING PARABOLIC AIRPLANE FLIGHT

ACKNOWLEDGMENT

The research described in this paper was carried out at the Jet Propulsion Laboratory, California Institute of Technology, under contract with the National Aeronautics and Space Administration.

REFERENCES

1. Okress, E.C., Wroughton, D.M., Comenetz, G., Bruce, P.A., and Kelly, J.C.R. "Electromagnetic levitation of solid and molten materials", J. Appl. Phys. **23**, 545-552 (1952)

2. Cummings, D.L., and Blackburn, D.A., "Oscillations of magnetically levitated aspherical droplets", J. Fluid Mech. **224**, 395-416 (1991)

3. Rhim, W.K. , Chung, S.K., Man, K.F., Gutt,G., Rulison, A. and Spjut, R.E., "An electrostatic levitator for high temperature containerless materials processing in 1 G", Rev. Sci. Instrum. **64**, 2961-2971 (1993)

4. Trinh, E.H. "Compact acoustic levitation device for studies in fluid dynamics and material science in the laboratory and microgravity", Rev. Sci. Instrum. **56**, 2059-2065 (1985), and E.H. Trinh, J. Robey, A. Arce, and M. Gaspar, "Experimental studies in fluid mechanics and materials science using acoustic levitation", Mat. Res.Soc. Symp. Proc. **87**, 57-69 (1987)

5. Gopinath, A and Mills, A.F., "Convective heat transfer from a sphere due to acoustic streaming", J. Heat Transfer, **115**, 332-341 (1993)

6. Leung, E.W., Baroth, E., Chan, C.K., and Wang, T.G.,"Thermal acoustical interaction and flow phenomenon", AIP Conference Proceedings **197**, 58-70, T.G. Wang Editor, New York, N.Y. (1989)

7. Fand, R.M. and Kaye, J., "The influence of sound on free convection from a horizontal cylinder", J. of Heat Transfer **83**, 133-148 (1961)

8. Fand, R.M. "Mechanism of interaction between vibrations and heat transfer", J. Acoust. Soc. Am. **34**, 1887-1894 (1962)

9. Trinh, E.H., "Levitation studies of the physical properties and nucleation of undercooled liquids", *Proc. VII European Symposium on Materials and Fluid Sciences in Microgravity*, ESA publication **SP-295**, 503-508 (1990)

THERMOACOUSTIC STREAMING EFFECTS FROM A SPHERE SUBJECT TO TIME-PERIODIC TEMPERATURE DISTURBANCES

Ashok Gopinath
Department of Physics, Naval Postgraduate School,
Monterey, CA 93943-5117, U.S.A.

Satwindar Singh Sadhal
Department of Mechanical Engineering, University of Southern California,
Los Angeles, CA 90089-1453, U.S.A.

ABSTRACT

The thermal analysis of the effect of the steady streaming motion induced by a solid sphere in an acoustic field is carried out by the singular perturbation method. For sufficiently large frequencies, a thin Stokes layer region on the surface of the sphere constitutes the inner solution for the flow field which is then matched with a suitable outer solution. The temperature field in the fluid is induced by a thermal oscillation on the sphere boundary while the ambient is held at a constant temperature. The interaction of the thermal oscillations and the acoustic field results in a nonzero time averaged steady convective transport of heat in the fluid. This is the principal effect being investigated in this study, with attention restricted to gases with Pr $\approx$ 1. As in the case of the velocity field, a singular perturbation procedure is employed for determining the temperature distribution in the fluid. For large streaming Reynolds numbers, R_s, being considered, the matching of the inner Stokes layer with the outer field is through a thicker outer boundary layer. While the inner solution can be found analytically, the outer solution requires numerical work. The final results show that although there is no net exchange of heat between the sphere and the fluid, there is, however, a steady flow of heat, into and out of, each hemisphere of the physical domain. This flow causes an equal heating and cooling of the fluid in each hemisphere, while within the solid sphere it is indicative of a steady temperature gradient across its poles.

NOMENCLATURE

a	Radius of the sphere
A	Oscillation amplitude of the sound wave, U_∞/ω
c	Velocity of propagation of sound in the fluid
M^2	Frequency parameter, $a^2\omega/\nu$
Nu_i	Inner average Nusselt number
Nu_0	Outer average Nusselt number
p_m	Mean fluid pressure
p_0	Acoustic pressure amplitude
Pr	Prandtl number
r	Radial coordinate, r^*/a
R_s	Streaming Reynolds number, $U_\infty^2/\omega\nu = \varepsilon^2 M^2$
t	Dimensionless temperature defined in §4
T	Dimensional temperature of the fluid
T_∞	Temperature of the ambient
$(\Delta T)_a$	Amplitude of temperature oscillations
u, v	"Artificial" velocities defined in §4
u_θ, u_r	Angular, radial velocity components
U_∞	Velocity amplitude in the sound wave, $A\omega$
x, y	Boundary layer coordinates defined in §4
z^*	Coordinate in the axial direction

Greek Letters

γ	Phase difference between oscillations
γ_0, γ_1	Phase angles defined in Eqs. 19 and 20
γ_r	Ratio of specific heats of the fluid
δ	Stokes layer thickness, $\sqrt{\nu/\omega}$
ε	Amplitude parameter, A/a
$\eta, \bar{\eta}$	Normal boundary layer coordinates
μ, θ	Angular coordinates, $\mu = \cos\theta$
λ	Wavelength of the sound field
ν	Kinematic viscosity of the fluid
τ	Dimensionless time, $\omega\tau^*$
ϕ, Φ	Dimensionless temp. diff., $(T - T_\infty)/(\Delta T)_a$
ψ, Ψ	Dimensionless stream function
ω	Angular frequency

Superscripts

$*$	Represents dimensional quantities

1. INTRODUCTION

In this study, we examine the process of convective heat transfer due to acoustic streaming induced by a sound field about an isolated sphere which is subject to time-periodic temperature fluctuations. The principal feature of interest in the present study is the energy transport phenomenon emanating from the time-

independent contribution of the convective term due to the interactions of the thermal oscillations with the acoustic field.

In previous studies (Gopinath & Mills, 1993, hereafter referred to as [I], and Gopinath, 1993) the steady heat transport due to the streaming motion was examined for the case of an isothermal sphere exchanging heat with an isothermal fluid. However, in the current study, although the fluid ambient is considered isothermal, the temperature of the sphere is taken to be time–periodic. Such a situation could arise in, say, a pulsed heating process (see Magill et al., 1987) or other inherently time–periodic heat transfer processes. The basic problem of the sphere treated here would help address the larger issue of the influence of acoustic fields on such processes. Unlike the work of Arpaci (1966, pp. 324–335), or more recently Khedari et al. (1992), who have considered the *conductive* transfer of heat in solid bodies subject to time–periodic temperature boundary conditions, the present work deals principally with the *convective* transport of heat due to steady thermoacoustic streaming effects in the fluid around the sphere.

The steady streaming motion in the fluid is taken to be induced around a rigid sphere of radius, a, by a standing acoustic field with a velocity distribution of the form, $U_\infty \cos(\omega\tau^*)\sin(2\pi z^*/\lambda)$. The development follows that of [I] wherein length scale arguments were used to treat the parameter ranges of $a\omega/c \ll 1$ and $\varepsilon = U_\infty/a\omega \ll 1$, for which the flow induced around the sphere can be assumed to be laminar and unseparated, with negligible compressibility effects. This also allows the governing equations to be treated by the method of matched asymptotic expansions with ε playing the role of a small perturbation parameter. Furthermore, only the high frequency range, $M^2 = a^2\omega/\nu \gg 1$, is considered, for which the streaming effects are most significant. For the above conditions, the basic flow field around the sphere was developed by Riley (1966) who showed that the steady flow field of interest can be divided into essentially two distinct regions — a thin, inner recirculating Stokes layer region in which an $O(\varepsilon U_\infty)$ streaming velocity originates to drive the steady flow in an outer region making up of the remainder of the domain. Stuart (1966) recognized that the strength of the steady flow in the outer region is governed by a streaming Reynolds number, $R_s = \varepsilon^2 M^2$, which can be uniquely determined from the driving acoustic signal (see [I]). In the present study, the acoustic signal is taken to be sufficiently strong so as to give rise to large R_s, for which the steady transport effects due to the streaming motion are most pronounced. Particular attention is given to cases in which the surrounding fluid is a gas with $\mathrm{Pr} = O(1)$. For large R_s, the outer steady flow has a boundary layer structure (Stuart, 1966), the behavior of which has been obtained in [I].

For purposes of simplicity the periodic temperature excursions of the sphere are taken to be harmonic (at a single frequency) and of the form, $T_\infty + (\Delta T)_a \cos(\omega\tau^* + \gamma)$. It is assumed that the amplitude of these oscillations, $(\Delta T)_a$, is small enough to neglect (as a first approximation) any interaction of the thermal and acoustic fields. Furthermore, it is also assumed that any high–intensity thermoacoustic effects as discussed by Gopinath (1993) are small. The validity of this assumption can be ensured if a suitably defined Eckert number is maintained small. More importantly, it must be noted that the angular frequency of the acoustic field, ω, is taken to be "tuned" to match that of the temperature oscillations, with allowance made for a possible difference in phase, γ. Such isoharmonic situations are of principal interest since the magnitude of the expected steady heat transport resulting from the interactions of these oscillations is the strongest for such cases. In general however, the procedure followed in this study can be extended to any arbitrary periodic temperature disturbance, after it is Fourier decomposed into its constituent frequencies.

2. GOVERNING EQUATIONS

For this axisymmetric problem, we describe the fluid motion by the Stokes stream function ($\psi \equiv \psi^*/U_\infty a^2$) in a spherical coordinate system, i.e.,

$$u_r = -\frac{1}{r^2}\frac{\partial\psi}{\partial\mu} \quad \text{and} \quad u_\theta = -\frac{(1-\mu^2)^{-\frac{1}{2}}}{r}\frac{\partial\psi}{\partial r}, \tag{1}$$

where $\mu = \cos\theta$. The dimensionless governing equations of momentum and energy for the fluid are,

$$\frac{\partial}{\partial\tau}(D^2\psi) + \frac{\varepsilon}{r^2}\left[\frac{\partial(\psi, D^2\psi)}{\partial(r,\mu)} + 2D^2\psi L\psi\right] = \frac{1}{M^2}D^4\psi, \tag{2}$$

and

$$\frac{\partial\phi}{\partial\tau} + \frac{\varepsilon}{r^2}\left[\frac{\partial(\psi,\phi)}{\partial(r,\mu)}\right] = \frac{1}{Pr\cdot M^2}\nabla^2\phi, \tag{3}$$

where the operators D^2, L and ∇^2 are defined as

$$D^2 = \frac{\partial^2}{\partial r^2} + \frac{(1-\mu^2)}{r^2}\frac{\partial^2}{\partial\mu^2}, \quad L = \frac{\mu}{(1-\mu^2)}\frac{\partial}{\partial r} + \frac{1}{r}\frac{\partial}{\partial\mu}, \tag{4}$$

and

$$\nabla^2 = \frac{1}{r^2}\frac{\partial}{\partial r}\left[r^2\frac{\partial}{\partial r}\right] + \frac{1}{r^2}\frac{\partial}{\partial\mu}\left[(1-\mu^2)\frac{\partial}{\partial\mu}\right] \tag{5}$$

The boundary conditions are

$$\phi = \cos(\tau+\gamma) \quad \text{and} \quad \psi = \frac{\partial\psi}{\partial r} = 0 \quad \text{at } r = 1 \tag{6}$$

$$\left.\begin{array}{rcl}\psi & \rightarrow & \frac{1}{2}r^2(1-\mu^2)\cos\tau \\ \phi & \rightarrow & 0\end{array}\right\} \quad \text{as } r\rightarrow\infty \qquad (7)$$

In this study we are concerned with the cases of $\varepsilon \ll 1$ and $M \gg 1$. This parameter range has been treated by Riley (1966) to develop a solution for the *flow-field* in terms of inner and outer complementary perturbation series expansions in powers of ε and $1/M$. It has been further supplemented in [I] with a treatment of the large R_s flow field and the associated heat transfer problem. Similar methods are used in the following sections with a focus on determining the additional steady thermoacoustic streaming phenomena introduced by the interaction of the oscillating thermal and acoustic fields. These methods call for perturbation expansions in the inner and outer regions.

3. THE INNER REGION

For large values of the frequency parameter, M, the basic oscillatory flow has a Stokes boundary layer on the surface of the sphere with a largely irrotational exterior region. The mechanics of this inner oscillatory shear layer region of dimensional thickness of $O(\delta)$ is best understood in terms of suitably defined Stokes boundary layer variables (Riley, 1966),

$$\eta = (r-1)\frac{M}{\sqrt{2}} \quad \text{and} \quad \Psi(\eta,\mu,\tau) = \frac{M}{\sqrt{2}}\psi(r,\mu,\tau) \qquad (8)$$

with $\Phi(\eta,\mu,\tau) \equiv \phi(r,\mu,\tau)$, in view of which the governing Eqs. (2)-(3) become,

$$\frac{\partial}{\partial\tau}\left(\frac{\partial^2\Psi}{\partial\eta^2}\right) + \varepsilon\left[\frac{\partial(\Psi,\partial^2\Psi/\partial\eta^2)}{\partial(\eta,\mu)} + \frac{2\mu}{1-\mu^2}\frac{\partial\Psi}{\partial\eta}\frac{\partial^2\Psi}{\partial\eta^2}\right] = \frac{1}{2}\frac{\partial^4\Psi}{\partial\eta^4} + O(\varepsilon M^{-1}, M^{-2}) \qquad (9)$$

$$\frac{\partial\Phi}{\partial\tau} + \varepsilon\left[\frac{\partial(\Psi,\Phi)}{\partial(\eta,\mu)}\right] + O(\varepsilon M^{-1}) = \frac{1}{2\cdot Pr}\left[\frac{\partial^2\Phi}{\partial\eta^2} + \frac{2\sqrt{2}}{M}\frac{\partial\Phi}{\partial\eta} + O(M^{-2})\right] \qquad (10)$$

The above equations can be made to satisfy only the inner boundary conditions on the sphere surface, namely,

$$\Psi = \frac{\partial\Psi}{\partial\eta} = 0 \quad \text{and} \quad \Phi = \cos(\tau+\gamma) \quad \text{at } \eta = 0 \qquad (11)$$

The solution for the stream function, Ψ, is sought in a perturbation expansion of the form,

$$\Psi = \Psi_0 + \varepsilon(\Psi_{1s} + \Psi_{1u}) + \ldots \qquad (12)$$

for which the leading order contribution was obtained by Riley (1966, Eq. 28) as,

$$\Psi_0 = \frac{3\sqrt{2}}{4}(1-\mu^2) \times \left[\sqrt{2}\,\eta\cos\tau - \cos(\tau-\frac{\pi}{4}) + e^{-\eta}\cos(\tau-\eta-\frac{\pi}{4})\right] \qquad (13)$$

Although the above form for Ψ_0 will suffice for the present study, it is important to note that it is the time-independent part of the $O(\varepsilon)$ contribution, Ψ_{1s}, (Riley, 1966, Eq. 32) which explains the behavior of the acoustic streaming motion in the inner region and provides a description of the slip-like velocity which drives the steady flow in the outer region.

For the temperature distribution also, a perturbation expansion of the form

$$\Phi = \Phi_0 + \varepsilon(\Phi_{1s} + \Phi_{1u}) + \ldots \qquad (14)$$

is sought. Here it can be shown from a solution of Eq. (3) subject to Eqs. (6)-(7) that the leading order solution, Φ_0, is given by

$$\Phi_0 = e^{-\eta\sqrt{\mathrm{Pr}}}\cos(\tau+\gamma-\eta\sqrt{\mathrm{Pr}}) \qquad (15)$$

and represents an oscillatory temperature wave in the Stokes layer region. Since the variation of Φ_0 is time-periodic, there is no net time averaged transfer of heat at this level. Of greater interest is the $O(\varepsilon)$ contribution to the temperature distribution in the fluid which arises only due to the presence of the acoustic field. An analysis of the $O(\varepsilon)$ balance of Eq. (10) using Eq. (14) shows that in addition to an $O(1)$ second harmonic and an $O(1/\sqrt{R_s})$ first harmonic contained in Φ_{1u}, there also arises from the convective term a non zero steady part, Φ_{1s}, resulting from the time-averaged interaction of the leading order oscillatory temperature and flow fields in the fluid. The behavior of this steady part is governed by

$$\frac{1}{2\,Pr}\frac{\partial^2\Phi_{1s}}{\partial\eta^2} = \left\langle\frac{\partial(\Psi_0,\Phi_0)}{\partial(\eta,\mu)}\right\rangle, \qquad (16)$$

where the angle-brackets, $\langle\ \rangle$, denote a time-average of the enclosed quantities. This equation is subject to the inner boundary condition

$$\Phi_{1s} = 0 \qquad \text{at } \eta = 0 \qquad (17)$$

and appropriate matching with the outer region. Although the details of the analysis have been excluded, it can be shown that the resulting variation of Φ_{1s} can be obtained from a solution of the above equations as,

$$\Phi_{1s} = \frac{3\mu}{2}e^{-\eta\sqrt{\mathrm{Pr}}}\left[\sqrt{\mathrm{Pr}}\,(1-\eta)\cos(\gamma-\eta\sqrt{\mathrm{Pr}}) - (2+\eta\sqrt{\mathrm{Pr}})\sin(\gamma-\eta\sqrt{\mathrm{Pr}})\right.$$

$$+ \quad \frac{\mathrm{Pr}\sqrt{\mathrm{Pr}}}{(1+\mathrm{Pr})^2} e^{-\eta} \left\{ (1-\mathrm{Pr}) \cos(\gamma + \eta - \eta\sqrt{\mathrm{Pr}}) \right.$$
$$\left. + \quad 2\sqrt{\mathrm{Pr}} \sin(\gamma + \eta - \eta\sqrt{\mathrm{Pr}}) \right\} \Big]$$
$$+ \quad \mu\, \Phi_{1\infty}(\mathrm{Pr}, \gamma) \qquad (18)$$

where

$$\Phi_{1\infty}(\mathrm{Pr}, \gamma) = \frac{3}{2} \frac{\sqrt{9\mathrm{Pr}+4}}{(1+\mathrm{Pr})} \sin(\gamma - \gamma_0)$$
$$\text{with} \quad \tan\gamma_0 = \frac{\sqrt{\mathrm{Pr}}(1+3\mathrm{Pr})}{2(1+2\mathrm{Pr})} \qquad (19)$$

There are two important implications of this steady temperature variation, both of which depend strongly on the phase difference, γ, namely :

(1) Equation (18) predicts a non-zero fluid temperature gradient at the sphere wall given by

$$\left.\frac{\partial \Phi_{1s}}{\partial \eta}\right|_{\eta=0} = \frac{3\mu}{\sqrt{2}} \sin(\gamma_1 + \pi/4) \sin(\gamma - \gamma_1)$$

with

$$\tan\gamma_1 = \frac{\sqrt{\mathrm{Pr}} - 1}{\sqrt{\mathrm{Pr}} + 1}. \qquad (20)$$

This yields an average *inner* Nusselt number (based on the sphere diameter) for the corresponding heat transfer rate over each hemisphere as,

$$\frac{Nu_i}{\sqrt{R_s}} = \int_0^1 \left(-\frac{\partial \Phi_{1s}}{\partial \eta} \right)_{\eta=0} d\mu$$
$$= -\frac{3}{2} \sin(\gamma_1 + \pi/4) \sin(\gamma - \gamma_1) \qquad (21)$$

(2) The variation in Eq. (19) also prescribes a temperature at the outer edge of the inner Stokes region ($\Phi_{1s}(\eta \to \infty) \to \mu\, \Phi_{1\infty}$) which in turn determines the steady temperature distribution in the outer region.

4. THE OUTER REGION, $R_s \gg 1$

For the related problem of the steady variation of velocity and temperature in the outer region, the solution in the form of series expansions similar to Eqs. (12) and (14) is sought. Therefore, the following expansions are used

$$\psi = \psi_0 + \varepsilon\, (\psi_{1s} + \psi_{1u}) + \ldots \qquad (22)$$
$$\phi = \phi_0 + \varepsilon\, (\phi_{1s} + \phi_{1u}) + \ldots \qquad (23)$$

with particular interest in the dominant contributions of the time-independent portions of each, namely the steady component of the $O(\varepsilon)$ term, ψ_{1s}, in Eq. (22) for the stream function and the $O(\varepsilon)$ term, ϕ_{1s}, in Eq. (23) for the temperature. For completeness it is also useful to quote the solution for the basic leading order contribution to the stream function, ψ_0 in Eq. (22), obtained by Riley (1966, Eq. 27) as,

$$\psi_0 = \frac{1}{2} r^2 \left(1 - \frac{1}{r^3}\right) (1 - \mu^2) \cos r \qquad (24)$$

For the leading order temperature, ϕ_0 in Eq. (23), matching (as $\eta \to \infty$) with the exponentially decaying oscillatory behavior of the inner region in Eq. (15) shows that in the outer region $\phi_0 \equiv 0$.

Stuart (1966) showed that the nature of the steady transport effects in the outer region is governed by the magnitude of the streaming Reynolds number, R_s. This parameter can be determined from the acoustic signal and the fluid properties as described (for the case of air) in Eqs. (13)-(16) of [I]. In general, for a plane standing acoustic field in an ideal gas, R_s can be expressed as

$$R_s = \frac{c^2}{\omega \nu \gamma_r^2} \left(\frac{p_0}{p_m} \right)^2 \qquad (25)$$

where (p_0/p_m) is the pressure amplitude ratio, which is oftentimes the measured parameter used to characterize strong acoustic fields.

For large values of R_s and $\mathrm{Pr} = O(1)$ being considered here, the variation of the steady terms ψ_{1s} and ϕ_{1s} in this outer region exhibits a boundary layer behavior (Stuart 1966), as mentioned before in §1. Although this boundary layer region is thin on the scale of the sphere radius, it is much thicker than the inner Stokes layer. This region has to be analyzed by a *numerical* solution of the governing equations subject to suitable matching conditions from the inner region. These equations themselves may be obtained in a manner described by Riley (1966). The process is not entirely trivial and the details have been omitted here. The relevant equations as developed in [I] have been summarized below in their final forms. The outer boundary layer variables are defined as,

$$\bar{\eta} = (r - 1)\sqrt{R_s} \qquad (26)$$

and

$$\bar{\psi}_{1s}(\bar{\eta}, \mu) = \psi_{1s}(r, \mu)\sqrt{R_s}, \quad \bar{\phi}_{1s}(\bar{\eta}, \mu) \equiv \phi_{1s}(r, \mu). \qquad (27)$$

For convenience these are expressed in terms of commonly used symbols for the coordinates and suitably defined "artifical" velocities,

$$y \equiv \bar{\eta} \ , \ x \equiv \mu \ , \ u = \frac{\partial \bar{\psi}_{1s}}{\partial \bar{\eta}} \ , \ v = -\frac{\partial \bar{\psi}_{1s}}{\partial \mu} \qquad (28)$$

along with

$$t(x,y) \equiv \bar{\phi}_{1s}(\mu,\bar{\eta}). \tag{29}$$

The governing equations in these variables are,

$$\frac{\partial u}{\partial x} + \frac{\partial v}{\partial y} = 0 \tag{30}$$

$$u\frac{\partial u}{\partial x} + v\frac{\partial u}{\partial y} + \frac{xu^2}{(1-x^2)} = \frac{\partial^2 u}{\partial y^2} \tag{31}$$

$$u\frac{\partial t}{\partial x} + v\frac{\partial t}{\partial y} = \frac{1}{Pr}\frac{\partial^2 t}{\partial y^2} \tag{32}$$

with boundary conditions

$$u = \frac{45}{16}x(1-x^2), \quad v = 0, \quad t = x\Phi_{1\infty} \text{ at } y = 0 \tag{33}$$

$$u \to 0, \quad t \to 0 \quad \text{as } y \to \infty \tag{34}$$

It may be recalled from the brief discussion at the end of §3, that the limiting value of the temperature from the inner region, $\Phi_{1\infty}$ in Eq. (19), prescribes the driving temperature for the outer region as is clear from the temperature boundary condition in Eq. (33).

The governing equations are now completely defined and can be solved with the help of a suitable numerical method. The coupled set of nonlinear partial differential equations for u and v are first solved using an implicit finite-difference scheme with marching of the solution from the equator ($x = 0$) to the poles ($x = \pm 1$). All the derivatives are approximated by central differences and the nonlinearity is handled by quasi-linearization and iteration at each x-station along the periphery. Owing to the decoupled nature of the momentum and energy equations, once u and v have been determined, the temperature, t, can be found in a relatively straightforward non-iterative manner using triangular resolution and backward substitution. The symmetry about the equatorial plane is exploited to carry out the procedure over only one hemisphere. Further details of the discretization scheme and the grid parameters as well as an account of the means of accomodating the converging flow in the polar regions may be found in [I].

It must be emphasized that the system of governing equations and boundary conditions presented above for the outer region, is strictly valid only for cases of strong streaming motion ($R_s \gg 1$) in moderate Prandtl number fluids ($Pr \sim 1$).

5. RESULTS AND DISCUSSION

It should be noted at the outset that the results for the steady flow field, ψ_{1s}, are known and a representative plot of the boundary layer velocity profiles may be found in Fig. 3 of [I]. It is the variation of the steady temperature and the related heat transfer effects which will be of special interest in this study.

A representative plot of the numerically determined outer boundary layer temperature profiles for air (Pr = 0.7) is given in Fig. 1 for the case of $(\gamma - \gamma_0) = \pi/2$ and $0° < \theta \leq 90°$. For the other hemisphere ($90° \leq \theta < 180°$), the sign on the temperature values is reversed and the corresponding distribution may be simply obtained by a reflection about the y-axis.

Also of interest, is the variation of the local heat flux over the periphery of the sphere. This is characterized by the local driving temperature gradient for the outer region, $(-\partial t/\partial y)_{y=0}$, which is plotted in Fig. 2, also for $Pr = 0.7$ and $(\gamma - \gamma_0) = \pi/2$. The observed trend in this figure may be explained as follows: since, according to Eq. (33), $t \sim x$, the magnitude of the temperature and its gradient increase with $|x|$ as the flow progresses from the equator to the poles. However, as the flow converges towards the poles ($x = \pm 1$), continuity dictates a thickening of the boundary layers. This in turn reduces the driving fluid temperature gradient, which becomes negligible as $x \to \pm 1$, where there is a breakdown of the boundary layer structure of the flow. The temperature gradient thus reaches a maximum at some intermediate angular location, which for air (Pr = 0.7), occurs at $\theta \approx 45°, 135°$. The resulting heat transfer rate with the fluid (over each hemisphere) can be characterized by an average *outer* Nusselt number (based on the sphere diameter) by numerically integrating this driving temperature gradient. For air (Pr = 0.7) this gives

$$\frac{Nu_0}{\varepsilon\sqrt{R_s}} = \int_0^1 \left(-\frac{\partial t}{\partial y}\right)_{y=0} dx \approx 1.20 \sin(\gamma - \gamma_0) \tag{35}$$

An observation of the μ-dependence of the temperature in Eqs. (18)-(20) (and hence in Eq. (33)) shows that the driving temperature and its gradient in both the inner and outer regions, are antisymmetric about the plane of the equator. This indicates that the Nusselt number results in Eqs. (21) and (35) are only valid for each hemisphere, and there is no net exchange of heat between the entire sphere and the fluid. Such a situation is physically realized in the *fluid* by an equal amount of cooling and heating in each hemispherical portion of the domain, while within the *solid* sphere it takes the form of a steady flow of heat into a hemisphere and out the other, across the equatorial plane. Thus in the sphere, this time averaged heat flow rate is capable of inducing a steady temperature gradient across its poles. It is also clear from these Nusselt number results that the magnitude and direction of this heat flow strongly depend on the relation between the imposed phase difference, γ, and the innate phasing provided by the fluid via γ_0 and

γ_1, which is a characteristic feature of such thermoacoustic flows. We are currently investigating the roles of the solid/fluid thermal properties in such a thermoacoustic interaction, for a physically more realistic situation where a controlled pulsating surface heat source (rather than a temperature source) as discussed by Magill et al. (1987) is applied.

In concluding, it is emphasized that this fundamental problem serves to underline the importance of the ability to induce steady heat transfer rates to/from a body subject to time-periodic temperature fluctuations. A suitably chosen acoustic field is an important participant here and without it, the body *does not* experience a *steady* exchange of heat with the surrounding fluid.

ACKNOWLEDGEMENTS

The authors are grateful for support provided by the National Research Council under the Research Associateships Program (to A.G.) and by NASA Headquarters (to S.S.S., Grant No. NAGW-3378).

REFERENCES

V. S. Arpaci. 1966, Conduction Heat Transfer, pp. 324-335, Addison-Wesley, Reading, Massachusetts.

A. Gopinath. 1993, Convective heat transfer from a sphere due to acoustic streaming : Effects of viscous dissipation and compressibility work, 29th Natnl. Heat Transfer Conf. , Atlanta, HTD vol. 248, pp. 9-21.

A. Gopinath and A. F. Mills. 1993, Convective heat transfer from a sphere due to acoustic streaming, J. Heat Transfer, vol. 115, pp. 332-341. (referred to as [I])

J. Khedari, P. Benigni, J. Rogez, and J. C. Mathieu. 1992, A solution of the heat conduction equation in the finite cylinder exposed to periodic boundary conditions : the case of steady oscillation and constant thermal properties, Proc. Roy. Soc., vol. A438, pp. 319-329.

J. Magill, F. Capone, R. Beukers, P. Werner, and R. W. Ohse. 1987, Pulsed laser heating of acoustically levitated microspheres under pressure, High Temps. - High Pressures, vol. 19, pp. 461-471.

N. Riley. 1966, On a sphere oscillating in a viscous fluid, Q. J. Mech. Appl. Math., vol. 19, pp. 461-472.

J. T. Stuart.1966, Double boundary layers in oscillatory viscous flows, J. Fluid Mech., vol.24, pp. 673-687.

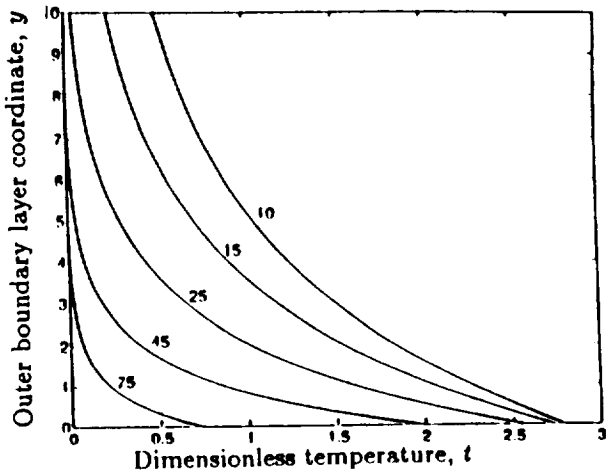

Figure 1. Outer boundary layer temperature profiles for air (Pr = 0.7) for the case of $(\gamma - \gamma_0) = \pi/2$ and large R_s. (The corresponding angular locations, θ, in degrees are shown on the figure)

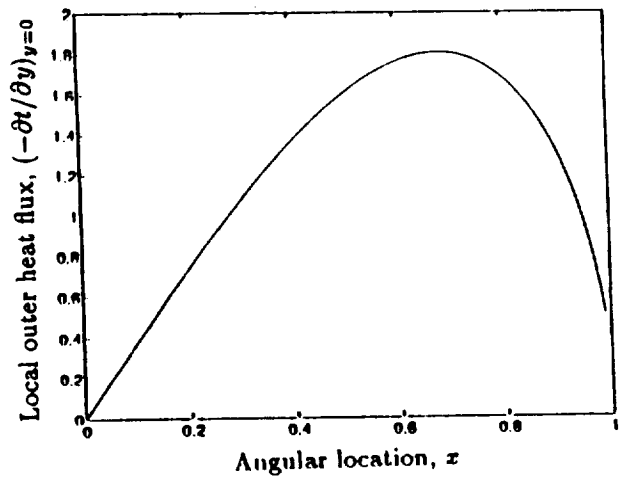

Figure 2. Distribution of the local outer heat flux for air (Pr = 0.7) over the upper hemisphere for the case of $(\gamma - \gamma_0) = \pi/2$ and large R_s.